J. Fluid Mech. (2024), *vol*. 999, A85, doi:10.1017/jfm.2024.883

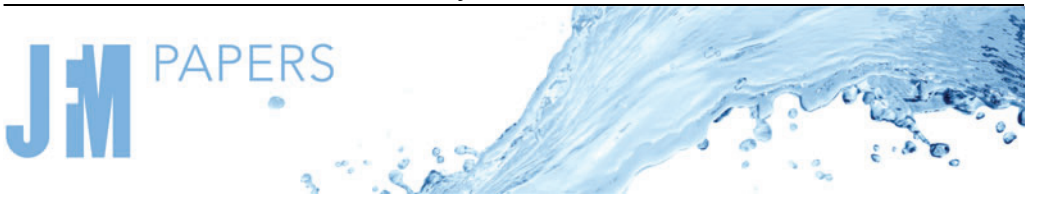

Formation and development of the stopping vortex ring in starting jets

Jianwei Zhu[1], **Guoqing Zhang**[1],†, **S.C.M. Yu**[2], **Lei Gao**[3] **and Ruijia Zhao**[1]

[1]Key Laboratory of Dynamics and Control of Flight Vehicle, School of Aerospace Engineering, Beijing Institute of Technology, Beijing 100081, PR China

[2]Department of Aeronautical and Aviation Engineering, The Hong Kong Polytechnic University, Kowloon, Hong Kong, PR China

[3]School of Aeronautics and Astronautics, Sichuan University, Chengdu 610065, PR China

(Received 1 March 2024; revised 18 August 2024; accepted 14 September 2024)

The formation mechanism for the stopping vortex ring (SVR) and its effects on the development of starting jets have been systematically investigated. The radial inward flow near the nozzle exit, arising from the pressure difference caused by the deceleration of starting jets, is considered to be the main contributing factor to the formation of the SVR. The formation process can generally be divided into (i) the rapid accumulation stage ($t_d^* \leq 1$) and (ii) the development stage ($t_d^* > 1$), where t_d^* is the formation time defined by the duration of the deceleration stage. For starting jets with different $(L/D)_d$, the final circulation value and circulation growth rate of the SVR can be scaled by $[(L/D)_d]^{-0.5}$ and $[(L/D)_d]^{-1.5}$, respectively. Here $(L/D)_d$ represents the stroke ratio during the deceleration stage. Analysing the temporal evolution of fluid parcels in the vicinity of the nozzle exit reveals that SVR entrains fluid from both inside and outside of the nozzle. Additionally, the influence of the SVR on the leading vortex ring and the trailing jet has been examined, with particular attention to its effects on the propulsive performance of the starting jet. The SVR affects the profiles of axial velocity and gauge pressure at the nozzle exit, thereby enhancing the generation of total thrust during the deceleration stage. Analysis has shown that depending on the deceleration rate, SVR can enhance the average velocity thrust by at least 10 % and compensate for up to a 60 % reduction in pressure thrust due to deceleration.

Key words: vortex dynamics, jets, vortex interactions

1. Introduction

A starting jet with finite discharged volume, known as a single-pulsed jet, is adopted by many aquatics in their propulsion systems, see for example jellyfish (Alben, Miller & Peng

† Email address for correspondence: zhanggq@bit.edu.cn

2013; Gemmell *et al.* 2013; Kang *et al.* 2023), squid (Anderson & Grosenbaugh 2005; Bi & Zhu 2020, 2022) and siphonophores (Costello *et al.* 2015; DuClos *et al.* 2022). Such starting jets, characterized by inherently unsteady characteristics, often provide significant thrust and enhance propulsive efficiency. This can be theoretically linked to the accompanying formation of vortical structures (Weihs 1977), especially the leading vortex ring (LVR) formed during the initial stage of a starting jet (Krueger & Gharib 2003, 2005; Gao *et al.* 2020; Zhang, Wang & Wan 2020). Previous investigations have also postulated that the optimal formation of the LVR is a unifying principle in the biological propulsion (Linden & Turner 2004; Dabiri 2009). In addition, it is worth noting that during the final deceleration stage of the starting jet, a relatively weaker vortex ring with an opposite sign to the LVR would be formed near the nozzle exit (Maxworthy 1977; Didden 1979; Auerbach 1991; Wakelin & Riley 1997).

Maxworthy (1977) and Didden (1979) were among the first to document the formation of a stopping vortex ring (SVR) near the nozzle exit during the final deceleration stage of the starting jet. This was attributed to the interaction between the nozzle wall and the induced flow from the LVR (c.f. figure 15 in Maxworthy (1977)). The experiments conducted by Auerbach (1991) and the numerical simulation by Wakelin & Riley (1997) also demonstrated the formation of the SVR. The SVR would draw back some of the vorticity from the trailing jet stem that has exited the nozzle exit (Wakelin & Riley 1997). The investigations mentioned above on the SVR all found that it moves upstream into the nozzle after being generated, and concurrently, the ring diameter of the LVR also decreases. For a starting jet released from an inclined nozzle, the SVR forms near the nozzle exit and connects to the LVR through a pair of vortex tubes (Troolin & Longmire 2010; Le *et al.* 2011). As the vortical structures interact, the SVR wraps around the LVR and contributes to its breakup. During the final deceleration stage of an annular starting jet, a pair of the SVRs with opposite signs could be found near the nozzle exit (Sadri & Krueger 2017; Zhu *et al.* 2022). At small stroke ratios L/D (the ratio of jet column length to diameter), this pair of the SVRs would push the LVR towards the central axis. Stopping vortex rings are also generated during the deceleration stage in each period of pulsed jets and interact with the LVR generated in the subsequent period (Asadi, Asgharzadeh & Borazjani 2018). For pulsed jets with different average non-dimensional periods, the SVR either maintains a ring shape or becomes unstable, forming hairpin vortices, to wrap around the LVR. It is worth noting that the SVR can also be observed in another method of generating vortex rings, i.e. the starting disk, which is an abstraction of a parachute (Higuchi, Balligand & Strickland 1996; Johari & Desabrais 2005) and partial drag-based propulsion (Ringuette, Milano & Gharib 2007; Fernando & Rival 2016). The SVR forms a pair of counter-rotating vortex rings with the LVR. This enables the LVR to move quickly away from the disk instead of following the disk under its self-induced velocity (Higuchi *et al.* 1996; Steiner *et al.* 2023).

In order to analyse the reasons for the difference between the analytical solution and the experimental results of the LVR generated by a starting jet, some investigations have attempted to suppress the formation of the SVR to eliminate its influence. This can be achieved, for example, by making the piston flush with the nozzle exit at the termination of its movement (Glezer 1988; Glezer & Coles 1990). Das, Bansal & Manghnani (2017) examined weakening the SVR by increasing the proportion of the impulse imparted by the piston during the deceleration stage to that during the entire duration of the starting jet. In their experiments, the velocity program of starting jet before deceleration remained unchanged, but only the duration of the deceleration stage was increased (c.f. figure 5 in Das *et al.* (2017)). The former implies that the strength of the LVR and its distance

from the nozzle exit remain unchanged, and the induced flow generated near the nozzle exit remains constant. However, prolonging the duration of the deceleration stage results in the weakening of the SVR. Similar conclusions can also be found in the numerical simulations by Gao *et al.* (2020). Therefore, it can be inferred that the flow near the nozzle exit induced by the LVR, as suggested by Maxworthy (1977) and Didden (1979), might not necessarily be the sole factor leading to the formation of the SVR. As shown above, previous investigations have not systematically studied the formation process and underlying mechanism of the SVR. Additionally, the quantitative influence from the SVR on the starting jet is yet to be addressed.

In the propulsion application of starting jets, the contribution of the SVR may be comparable to that of the LVR. During the swimming process of jellyfish, the formation of the SVR during the recovery stroke was first observed by Dabiri *et al.* (2005*a*,*b*). This vortex ring is equal in strength but with opposite sign to the LVR formed during the power stroke. In reality, the SVR and the LVR (generated in next swimming cycle) merge to form a laterally oriented vortical superstructure, which is critical as a flow source for the feeding and propulsion of jellyfish (Dabiri *et al.* 2005*a*). The interaction between these two vortex rings, including the cancellation of their opposite-signed vorticity, reduces the kinetic energy of rotational motion in the wake. As a result, the propulsive efficiency can be improved. Therefore, the SVR is considered to be a critical section in achieving passive energy recovery (Gemmell *et al.* 2013). Based on the force model developed for jellyfish swimming, Dabiri, Colin & Costello (2007) suggested that some jellyfish species may appear to violate the constraints imposed by their available muscle capabilities if the SVR is neglected.

As for the mechanically generated starting jet by the piston–cylinder apparatus, the strength of the observed SVR is much smaller than that of the LVR (Maxworthy 1977; Didden 1979; Auerbach 1991; Wakelin & Riley 1997), which is a marked difference compared with that generated by jellyfish. However, our recent investigations highlight that the influence of the SVR on the propulsive characteristics of mechanically generated starting jets cannot be neglected either (Gao *et al.* 2020; Zhu *et al.* 2024). Firstly, it was found that the induced velocity from the SVR would result in a region with positive gauge pressure at the nozzle exit after the termination of a starting jet. This contributes to the generation of positive pressure thrust, i.e. the integral of the gauge pressure profile at the nozzle exit. Secondly, it was also found that the SVR would affect the generation of thrust during the deceleration stage of a starting jet. The SVR near the nozzle edge acts as an obstacle, which causes the starting jet to contract towards the centreline. This is similar to the *vena contracta* (Limbourg & Nedić 2021*a*,*b*; Zhu *et al.* 2023*a*) in the starting jet generated by an orifice configuration. The contraction effectively reduces the effective flow cross-sectional area of the starting jet, thereby increasing the pressure at the nozzle exit. However, quantitative investigations into the influence of SVR on the transient evolution of propulsive quantities have yet to be undertaken. In addition, the influence of SVR on the thrust component generated by the momentum flux has not been considered previously.

The purpose of the present work is twofold. The first objective is to systematically study the formation process of the SVR. The key is to explore the underlying mechanism for its formation. The second objective is to systematically and quantitatively examine the influence of the SVR on the mechanically generated starting jet. This includes its influence on the two main components of a starting jet, i.e. the LVR and the trailing jet, as well as the transient evolution of propulsive quantities. A description of the physical problem for the present work and the numerical method adopted are introduced in § 2.

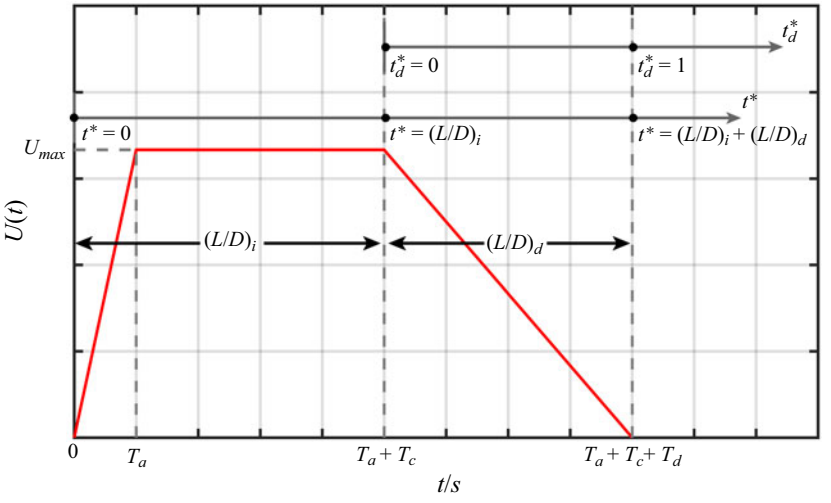

Figure 1. Schematic of the trapezoidal velocity program used to generate starting jets.

The results obtained in the present work and the related discussions are presented in §§ 3 and 4. Section 3 concentrates on the formation process of the SVR and the corresponding underlying mechanisms, while the influence of the SVR on the development of starting jet is specifically discussed in § 4. A brief summary in § 5 concludes the present work.

2. Physical problem and numerical method

The formation mechanism and role of the SVR formed during the deceleration stage of a starting jet will be studied in the present work. The key is to explore the factors responsible for the formation of the SVR and to distinguish the influence from the LVR. It can be inferred from Das *et al.* (2017) that as the duration of the deceleration stage is extended, SVR generated would be weakened. Therefore, the deceleration stage of the velocity program used to generate starting jets needs to be adjustable. Similar to Das *et al.* (2017), a simple trapezoidal velocity program (Rosenfeld, Rambod & Gharib 1998) shown in figure 1 is adopted, i.e.

$$U(t) = \begin{cases} U_{max}\dfrac{t}{T_a} & 0 \le t < T_a, \\ U_{max} & T_a \le t < T_a + T_c, \\ U_{max}\dfrac{T_a + T_c + T_d - t}{T_d} & T_a + T_c \le t < T_a + T_c + T_d, \\ 0 & T_a + T_c + T_d \le t, \end{cases} \tag{2.1}$$

where t is the physical time since the initiation of a starting jet, U_{max} is the velocity of starting jet before deceleration, while T_a, T_c and T_d denote the durations of the acceleration, constant velocity and deceleration stages, respectively. Two series of cases with different $(L/D)_i$ are compared, where $(L/D)_i$ is the stroke ratio before the starting jet begins to decelerate (see figure 1), i.e.

$$(L/D)_i = \frac{\displaystyle\int_0^{T_a+T_c} U(t)\,\mathrm{d}t}{D}, \tag{2.2}$$

Case	Re	Tip angle (°)	$(L/D)_i$	$(L/D)_d$
1–5	2000	7	0.75	0.125, 0.25, 0.5, 1, 2
6–10	2000	7	2.25	0.125, 0.25, 0.5, 1, 2
11, 12	2000	90	0.75	0.125, 1
13, 14	2000	90	2.25	0.125, 1
15–19	4000	7	0.75	0.125, 0.25, 0.5, 1, 2
20–24	4000	7	2.25	0.125, 0.25, 0.5, 1, 2

Table 1. Summary of the velocity program parameters and corresponding geometries for all cases adopted in the present work.

where D is the diameter of exit for the nozzle forming the starting jet. The LVR translates away from the nozzle exit under the self-induced velocity (Didden 1979). This allows the distance from the LVR to the nozzle exit to be different when SVR begins to form at different $(L/D)_i$, so that the influence from the LVR can be greatly weakened. In order to avoid possible influence due to different acceleration stages, T_a is kept constant, and different $(L/D)_i$ values are obtained only by varying T_c. The duration of the deceleration stage can also be expressed in terms of stroke ratio, as follows:

$$(L/D)_d = \frac{\int_{T_a+T_c}^{T_a+T_c+T_d} U(t)\,\mathrm{d}t}{D}. \tag{2.3}$$

For laminar vortex rings, the formation process of the LVR should be independent of the Reynolds number Re from 1250 to 5000 (Rosenfeld *et al.* 1998; Gao 2011), defined by

$$Re = \frac{\rho U_{max} D}{\mu}, \tag{2.4}$$

where ρ and μ are the density and dynamic viscosity of the fluid, respectively. Two different Re are considered for the formation process of the SVR.

In addition, the nozzle exit with and without a vertical wall is usually used to compare the formation process of a starting jet, as the induced flow would produce a stronger secondary boundary layer on the vertical wall than in the case without a vertical wall (Irdmusa & Garris 1987; Gharib, Rambod & Shariff 1998). The sign of the vorticity in the secondary boundary layer is consistent with that in SVR, so that it appears to contribute to the formation of SVR. This would be further examined in the present work, and the two nozzle exit geometries are compared, i.e. the cylindrical nozzle with a tip angle of 7° (Zhu *et al.* 2023*b*) and that with a vertical wall (90°). The velocity program parameters and corresponding geometries for all cases adopted in the present work are summarized in table 1, where the stroke ratio during the acceleration stage is maintained at 0.25 for all cases.

As for the formation time, the most commonly used form for the LVR is suggested by Gharib *et al.* (1998) and Pawlak *et al.* (2007) based on the definition of stroke ratio, as follows:

$$t^* = \begin{cases} \dfrac{\int_0^t U(t)\,\mathrm{d}t}{D} & 0 \le t < T_a + T_c + T_d, \\ \dfrac{\bar{U}t}{D} & t \ge T_a + T_c + T_d, \end{cases} \tag{2.5}$$

where $\bar{U}$ is the average velocity during the duration of starting jet, i.e.

$$\bar{U} = \frac{\int_0^{T_a+T_c+T_d} U(t)\,\mathrm{d}t}{T_a + T_c + T_d}, \tag{2.6}$$

where $\int_0^{T_a+T_c+T_d} U(t)\,\mathrm{d}t$ can also be considered as the length of the fluid column discharged by the starting jet. This can be related to the L/D of the starting jet, the sum of $(L/D)_i$ and $(L/D)_d$, that determines the generation of circulation (Gharib *et al.* 1998; Zhu *et al.* 2023*b*). Therefore, from a physical perspective, the circulation-related results shown in the present work, such as circulation, vorticity and vorticity flux, are normalized by $\bar{U}$. For easier analysis of the influence from the SVR, other results are normalized by U_{max}, which is the velocity before the deceleration of the starting jet and is the same for cases with the same Re. Furthermore, a new formation time can also be defined, taking into account the duration of deceleration stage T_d, which seems more suitable for the SVR in subsequent discussions, i.e.

$$t_d^* = \frac{t - T_a - T_c}{T_d}, \tag{2.7}$$

and the instant when SVR begins to form corresponds to $t_d^* = 0$. For cases with different $(L/D)_i$, $(L/D)_d$ and Re, the deceleration stage and the termination stage of the starting jet can be uniformly represented as $0 < t_d^* \leq 1$ and $t_d^* > 1$, respectively. For the same U_{max} in the velocity program (see (2.1)), the same formation time t_d^* in cases with different $(L/D)_i$ and $(L/D)_d$ also corresponds to the same velocity of a starting jet.

The present investigation is conducted using three-dimensional numerical simulations, where the computational domain for simulating the starting jet produced by a nozzle is an axisymmetric cylinder (Zhang *et al.* 2020; Zhu *et al.* 2022). For convenience, the cylindrical coordinate system (x, r, θ) is adopted to describe the cylindrical computational domain, with the origin located at the centre of the nozzle exit and the x-axis coinciding with the nozzle axis. One of the x–r planes passing through the x-axis is schematically shown in figure 2. Notably, all calculated results given subsequently are obtained by averaging values from four x–r planes at $\theta = 0°$, $90°$, $180°$ and $270°$. The variation between the results calculated for the SVR on the four x–r planes is much less than 1 %. Therefore, it can be considered that SVR is also axisymmetric, similar to the LVR (Limbourg & Nedić 2021*a*; Zhu *et al.* 2022). For the region downstream of the nozzle exit, the computational domain extends $15D$ in the axial direction and $5D$ in the radial direction. In addition, for the case of the nozzle with a tip angle of $7°$, the distance from the nozzle exit to the upstream outer boundary is $5D$. It has been confirmed by Zhu *et al.* (2023*a*) that the size of computational domain is sufficiently large so that the outer boundaries do not affect the development of a starting jet. The outer boundaries of the computational domain are composed of the slip boundary and the pressure outlet boundary. As for the nozzle generating the starting jet, it is a tube formed by the no-slip boundary with a length of $5D$. The vertical wall within the nozzle exit plane is also simulated with the no-slip boundary, as shown in figure 2(*b*) ($x = 0$, $0.5D \leq r \leq 5D$). The motion of the piston used to generate the starting jet in the experiment could be replaced by the velocity inlet boundary ($x = -5D$, $0 \leq r \leq 0.5D$) in the numerical simulation (Wakelin & Riley 1997; Rosenfeld *et al.* 1998; Gao *et al.* 2020; Zhu *et al.* 2022, 2023*a*). A time-dependent velocity program is prescribed at the velocity inlet boundary based on (2.1).

Similar to Zhu *et al.* (2022), the finite-volume-based computational fluid dynamics software package ANSYS Fluent 2021.R1 is used to numerically solve the unsteady,

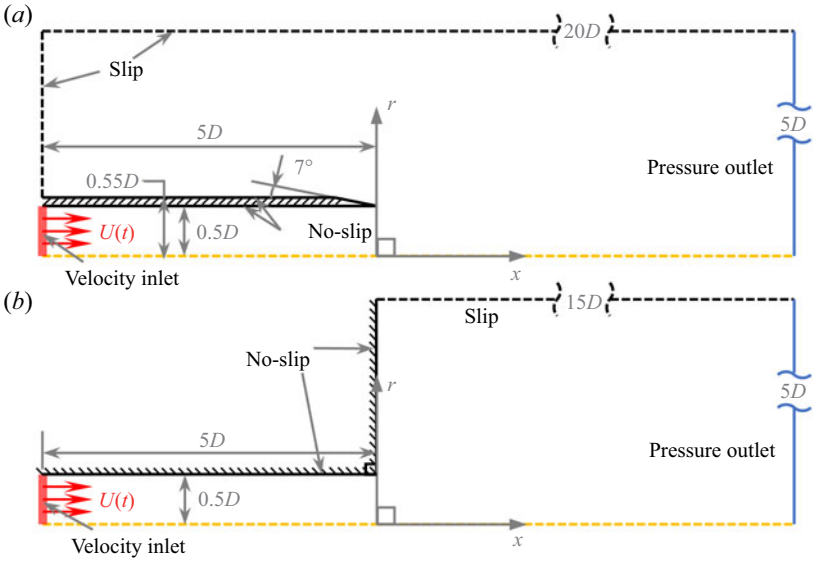

Figure 2. Schematic of the cylindrical computational domain and boundary conditions shown in the x–r plane for (a) the nozzle with a tip angle of 7° and (b) that with vertical wall.

incompressible Navier–Stokes equations for all cases. The PISO (pressure-implicit with splitting of operator) scheme, which is recognized for its suitability in unsteady simulation (Zhu *et al.* 2023*b*), is adopted to deal with the pressure–velocity coupling in incompressible equations. For the spatial discretization of equations, the least squares cell-based, second-order and bounded-central differencing methods are used for gradient, pressure and momentum discretization, respectively. As for the time advancement of the unsteady equations, the bounded second-order implicit method is employed. The reliability of the results obtained through the above numerical method in solving the formation process of the starting jet and the interaction of vortex rings has been verified in Zhu *et al.* (2022, 2023*a*,*b*) through comparison with experimental results.

The cylindrical computational domain is discretized using a non-uniform hexahedral structured grid scheme, with the finest grids concentrated in regions where shear layer and boundary layer are present, as shown in figure 3. The cylindrical region near the nozzle exit ($-0.6D \leq x \leq 4D$, $r \leq D$) is refined to enhance the accuracy of calculating the formation processes of the starting jet and SVR. For the grid independence test, two groups of grid schemes with three different degrees of refinement and the same grid topology are selected for the nozzle with a tip angle of 7° and the nozzle with a vertical wall, respectively. Both cases, the nozzle with a tip angle of 7° and the nozzle with a vertical wall, are also tested for time convergence. The velocity program for the starting jet used in the grid independence and time convergence tests is adopted from Case 15, which features the maximum rate of deceleration and higher Re. Similar to those used by Gao *et al.* (2020) and Zhu *et al.* (2022, 2023*a*,*b*), the circulation of the SVR (denoted as Γ_{SVR}) is calculated and compared at $t_d^* = 2$. The circulation can be obtained by integrating the azimuthal component of vorticity ω_θ within the vortex core area, i.e.

$$\Gamma = -\int \omega_\theta \, \mathrm{d}A, \tag{2.8}$$

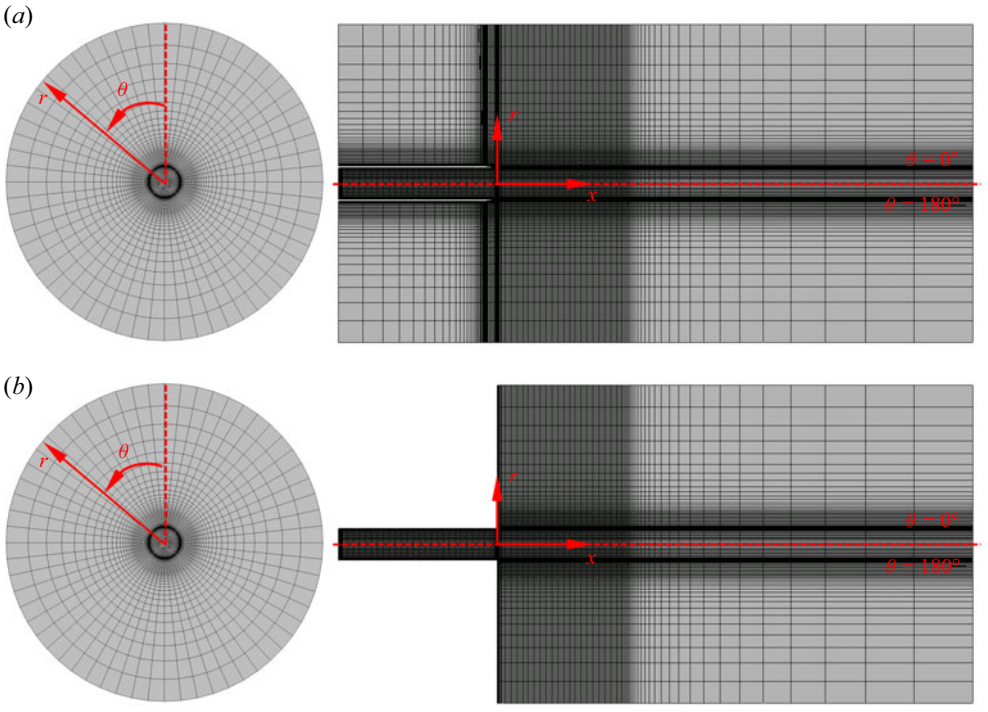

Figure 3. The grid used to discretize the computational domain in the r–θ and x–r planes for (a) the nozzle with a tip angle of 7° and (b) that with vertical wall. For clarity, the grid is coarsened while maintaining the same topology.

where the negative sign adopted after integration is due to the fact that the sign of ω_θ within SVR is negative, calculated as follows:

$$\omega_\theta = \frac{\partial v}{\partial x} - \frac{\partial u}{\partial r}, \tag{2.9}$$

where v and u are the components of the velocity in the r-axis and x-axis directions, respectively. The vortex core area can be identified using the Q-criterion (da Silva & Pereira 2008; Bi & Zhu 2020; de Guyon & Mulleners 2021), where Q can be calculated by

$$Q = -\frac{1}{2}\left[\left(\frac{\partial u}{\partial x}\right)^2 + \left(\frac{\partial v}{\partial r}\right)^2\right] - \frac{\partial u}{\partial r}\frac{\partial v}{\partial x}. \tag{2.10}$$

The vortex core area corresponding to SVR in the x–r plane with Q greater than 5 % of its maximum value is used for integration (c.f. the region with green boundary in figure 6b). The next paragraph then examines the sensitivity of the vortex core boundary determination method. The parameters and results for the grid independence and temporal convergence tests are summarized in table 2. With the refinement of the grid scheme and the shortening of the time step adopted in the present work, the difference in the circulation of the SVR is less than 1 %. Therefore, the grid schemes with 6 644 004 cells for nozzle with a tip angle of 7° and 5 766 324 cells for nozzle with a vertical wall, along with the time step of $\triangle t_d^* = 0.04$, are sufficient for the simulations in the present work.

Similar to Marugan-Cruz, Rodriguez-Rodriguez & Martinez-Bazan (2013), the vortex core boundary determination method used to calculate the circulation of the SVR is to be

	Tip angle (°)	Grid cells	$\triangle t_d^*$	$\frac{\Gamma_{SVR}(t_d^*=2)}{\bar{U}D}$	Relative error (%)
Grid independence	7	6 644 004	0.04	0.185250	—
		8 765 628	0.04	0.184786	0.251
		12 778 465	0.04	0.183893	0.733
	90	5 766 324	0.04	0.104679	—
		7 697 148	0.04	0.104750	0.068
		11 255 265	0.04	0.104286	0.375
Temporal convergence	7	6 644 004	0.04	0.185250	—
		6 644 004	0.02	0.186036	0.424
		6 644 004	0.01	0.186750	0.810
	90	5 766 324	0.04	0.104679	—
		5 766 324	0.02	0.104857	0.176
		5 766 324	0.01	0.104964	0.273

Table 2. Summary of the parameters and results for the grid independence and temporal convergence tests. The calculation of relative errors is based on the results obtained using the grid scheme and time step employed in the present work.

tested for its sensitivity to variations in the threshold. The circulation of the SVR in Case 15 is calculated at $t_d^* = 0.5$ and $t_d^* = 2$ using the region where Q exceeds 1 % to 10 % of its maximum value. The calculation results are shown in figure 4(*a*). The circulation of the SVR calculated decreases approximately linearly with increasing the selected threshold. When the threshold increases from 1 % to 10 % of the maximum value of Q, the circulation decreases by approximately 10 % at both $t_d^* = 0.5$ and $t_d^* = 2$. This is determined by the vorticity distribution in the vortex core (Kaplanski *et al.* 2009). Therefore, a smaller threshold results in an SVR circulation calculation that can more completely detect the vortex core area of the SVR. However, a threshold that is too small may result in the inclusion of additional regions in the circulation calculation, rather than just the vortex core area of the SVR. This is also why the circulation calculated anomaly decreases at $t_d^* = 0.5$ when the threshold is reduced from 2 % to 1 % of the maximum value of Q. The azimuthal vorticity contours near the nozzle exit at $t_d^* = 0.5$ and $t_d^* = 2$ are shown in figures 4(*b*) and 4(*c*), along with the vortex core boundaries for the SVR determined by different thresholds of Q. At $t_d^* = 0.5$, it is observed that using 1 % of the maximum value of Q as the threshold includes part of the positive vorticity region that originally belongs to the starting jet. This problem can be circumvented by increasing the threshold to 5 % or 10 % of the maximum value of Q. Of course, at $t_d^* = 2$, due to the full development, the vortex core region of the SVR can be captured more accurately, even with 1 % of the maximum value of Q as the threshold. To accurately track the variation of circulation during the formation and development processes of SVR, a consistent threshold should be applied to determine its boundary. In comparison, using 5 % of the maximum value of Q as the threshold seems to be better. It is small enough and does not mistakenly capture other regions in the initial formation process of the SVR.

Whether increasing $(L/D)_i$ from 0.75 to 2.25 can effectively eliminate the influence of the LVR on the formation process of SVR near the nozzle exit needs to be verified. As $(L/D)_i$ increases, the LVR does translate downstream and away from the nozzle exit, but its intensity increases by absorbing more fluid and vorticity and enhances the influence. The formation and kinematics of the SVR may be affected by the straining field (Trieling, Beckers & Van Heijst 1997) induced by the LVR. Due to the axisymmetry of the flow, the

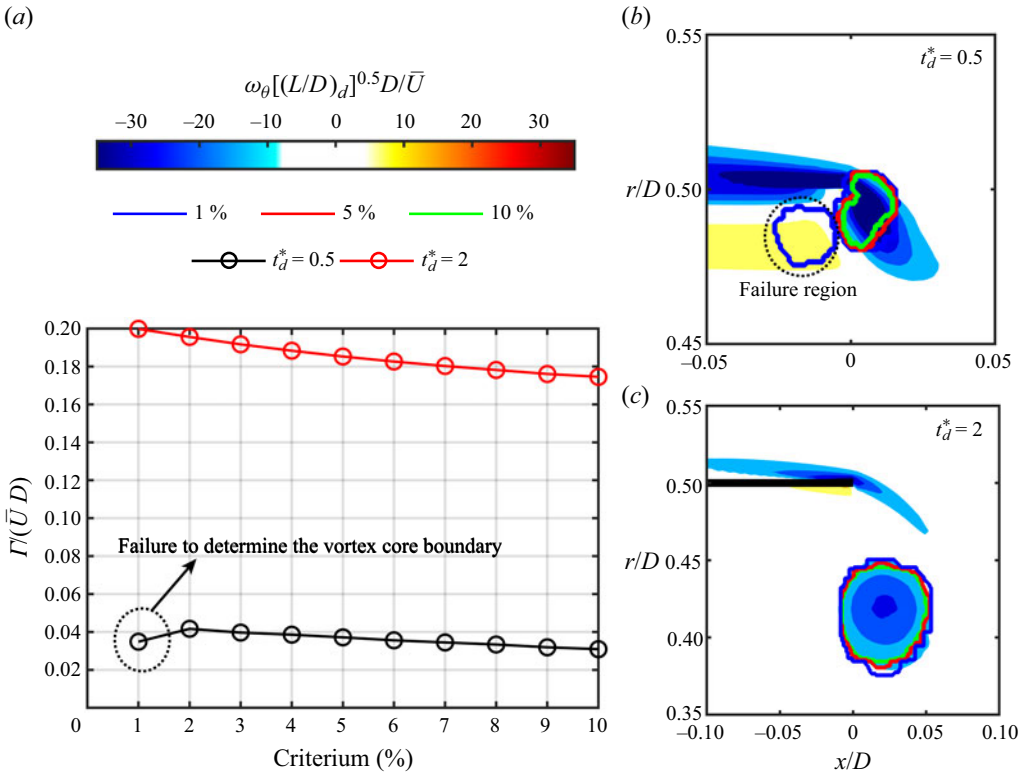

Figure 4. Sensitivity test of the vortex core boundary determination method. (*a*) Variation of the SVR circulation calculated with the vortex core boundaries determined by different critical values of Q, as well as azimuthal vorticity contours near the nozzle exit and the vortex core boundaries for the SVR determined by different thresholds of Q in Case 15 at (*b*) $t_d^* = 0.5$ and (*c*) $t_d^* = 2$.

straining field can be calculated in the x–r plane as follows:

$$\boldsymbol{e} = \frac{\partial u}{\partial x}\boldsymbol{i} + \frac{\partial v}{\partial r}\boldsymbol{j}, \tag{2.11}$$

where $\boldsymbol{i}$ and $\boldsymbol{j}$ represent the unit vectors in the x-axis and r-axis directions, respectively. The straining field near the nozzle exit in cases with different $(L/D)_i$ is shown in figure 5 for the instant of $t_d^* = 0$, i.e. the initial instant of the SVR formation. For smaller $(L/D)_i$, the straining field induced by the LVR dominates the nozzle exit where SVR is about to form, as shown by the blue isolines in figures 5(*a*) and 5(*b*). As $(L/D)_i$ increases, the region with higher strain magnitudes does indeed expand, but its downstream movement has indeed reduced its influence on the area near the nozzle exit. Compared with the case with $(L/D)_i = 0.75$, the influence of the straining field induced by the LVR at the nozzle exit can be approximately ignored in that with $(L/D)_i = 2.25$ (figure 5*d*), which means that the subsequent formation process of the SVR can be relatively independent from the influence of the LVR.

Furthermore, attention is directed to the instantaneous profiles of radial velocity v at the nozzle exit for cases with different $(L/D)_i$, as shown in figure 6, which directly reflect the flow induced by the LVR and the possibly trailing vortex. The results at $t_d^* = 0$ are given, at which point the deceleration factors mentioned later do not yet exist. It can be found that in the region outside the starting jet, i.e. $r > 0.5D$, there is a non-negligible radial inward flow

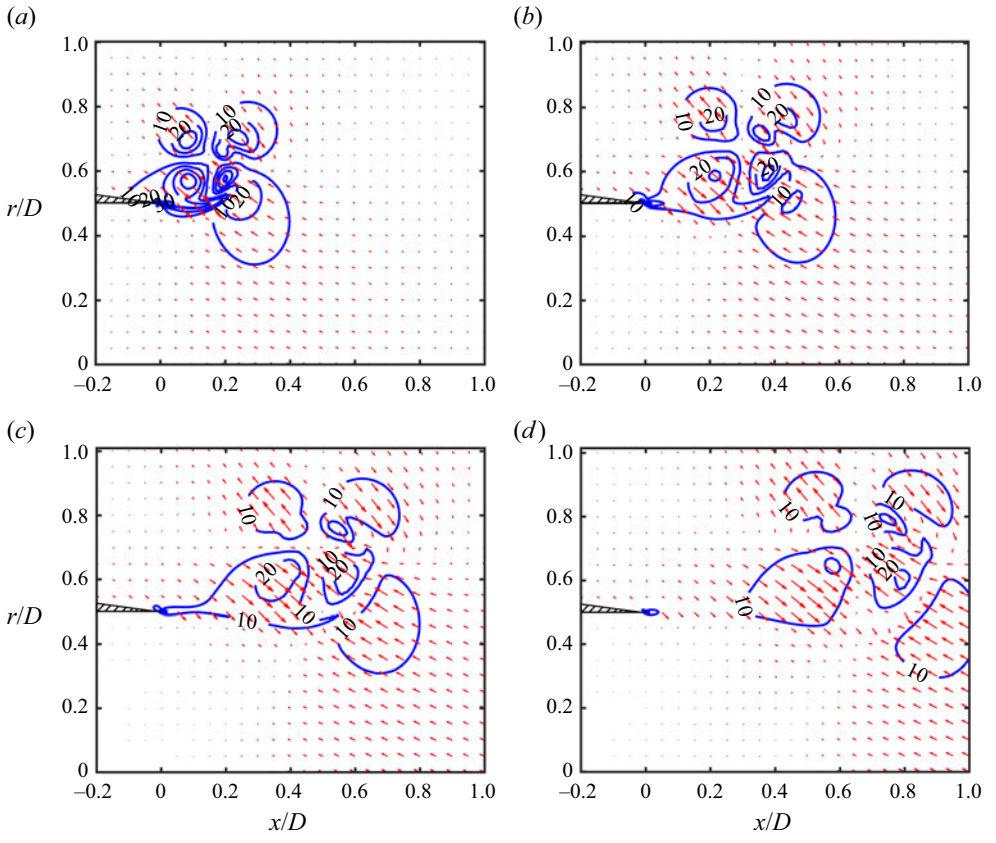

Figure 5. The straining field near the nozzle exit in cases with different $(L/D)_i$ at $t_d^* = 0$, where the solid blue lines represent the isolines of strain magnitude: (*a*) $(L/D)_i = 0.75$; (*b*) $(L/D)_i = 1.25$; (*c*) $(L/D)_i = 1.75$; (*d*) $(L/D)_i = 2.25$.

before the initiation of deceleration. This can be attributed to the flow induced by the LVR (Maxworthy 1977) and the possibly trailing vortex, or to the entrainment associated with the starting jet (Olcay & Krueger 2010). This radially inward flow is effectively weakened as $(L/D)_i$ increases. The magnitude of the maximum v at $(L/D)_i = 2.25$ is reduced to one-quarter of that at $(L/D)_i = 0.75$. As will be discussed later, the circulation of the SVR is not reduced so significantly but only by 10 %. The effective weakening of the radial inward flow by increasing $(L/D)_i$ remains at different *Re*, comparing figures 6(*a*) and 6(*b*).

3. Formation process of the SVR

3.1. *Formation mechanism*

The formation process of the SVR can be roughly divided into two stages based on its vorticity distribution: the rapid accumulation stage ($t_d^* \leq 1$) and the development stage ($t_d^* > 1$). The azimuthal vorticity contours near the nozzle tip during the initial formation process in Cases 1 and 4 are shown in figure 7. Based on the right-hand rule, the azimuthal vorticity ω_θ in the trailing shear layer and LVR of the starting jet is designated as positive (anticlockwise), whereas ω_θ in SVR is negative (clockwise). For $t_d^* \leq 1$, the negative vorticity accumulates rapidly at the nozzle tip ($x = 0$, $r = 0.5D$) with a concentrated

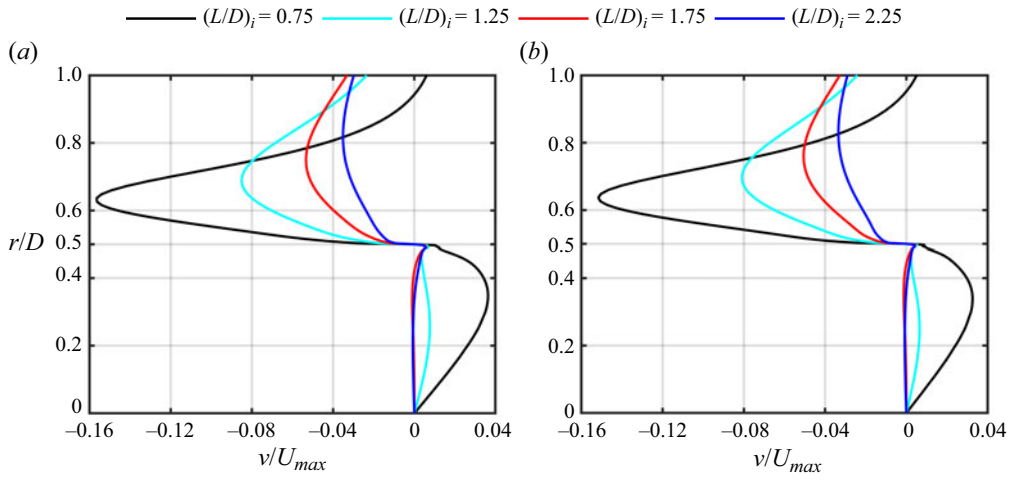

Figure 6. The instantaneous profiles of the velocity component in the r-axis direction, v, at the nozzle exit in cases with different $(L/D)_i$ at $t_d^* = 0$, where (*a*) $Re = 2000$ and (*b*) $Re = 4000$.

vorticity distribution, as shown in figures 7(*a*), 7(*b*), 7(*d*) and 7(*e*). During this stage, the vortex core of the SVR does not develop an independent maximum point of local vorticity magnitude; instead, the maximum point consistently remains located at the nozzle tip ($x = 0$, $r = 0.5D$). Subsequently, the development of the SVR rearranges the initially concentrated vorticity distribution into an approximately Gaussian distribution (Kaplanski *et al.* 2009) within the vortex core at $t_d^* > 1$, as shown in figures 7(*c*) and 7(*f*). The maximum point of local vorticity magnitude then appears at the centre of the vortex core of the SVR. The vortex core of the SVR begins to move away from the nozzle tip. This, in turn, induces a small positive vorticity region near the nozzle wall. The two phenomena observed after the termination of the starting jet can also be interpreted as breaking away from the spatial confinement imposed by the axial flow of the starting jet. The two stages during the formation of the SVR can be roughly distinguished at $t_d^* = 1$. This seems to be independent of the duration of the deceleration stage, i.e. $(L/D)_d$. The only variation observed is that SVR weakens as $(L/D)_d$ increases, comparing figures 7(*c*) and 7(*f*).

The vorticity contours and Q-criterion visualizations for Case 1 are further shown over a longer time period with larger spatial scale in figure 8. Also shown in the figure are the results obtained by the fluid tracer method (Yang, Jia & Yin 2012). It can be seen from figure 8(*a* i) that before the starting jet begins to decelerate ($t_d^* = 0$), a secondary boundary layer with negative vorticity, induced by the flow from the LVR (Irdmusa & Garris 1987), appears outside the nozzle tip. As the starting jet decelerates ($t_d^* > 0$), the negative vorticity rapidly accumulates in this region, especially near the nozzle tip (figure 8*b* i). The Q-criterion also clearly indicates that the vortical structure begins to appear near the nozzle tip (figure 8*b* ii). This shows the existence of the SVR, i.e. the red region bounded by green. At the same time, the trailing shear layer of the starting jet also bends radially inward towards the centre line. The most critical is that for Case 1 with $(L/D)_i = 0.75$, the LVR does not have enough time to translate away from the nozzle exit, where SVR is located. Consequently, the LVR and SVR form a pair of vortex rings with opposite signs, generating the mutually induced velocities (Zhu *et al.* 2022). The SVR translates downstream and reduces the radial position of the vortex core due to the mutually induced velocity from the LVR (indicated by the red arrow on the SVR), even though the

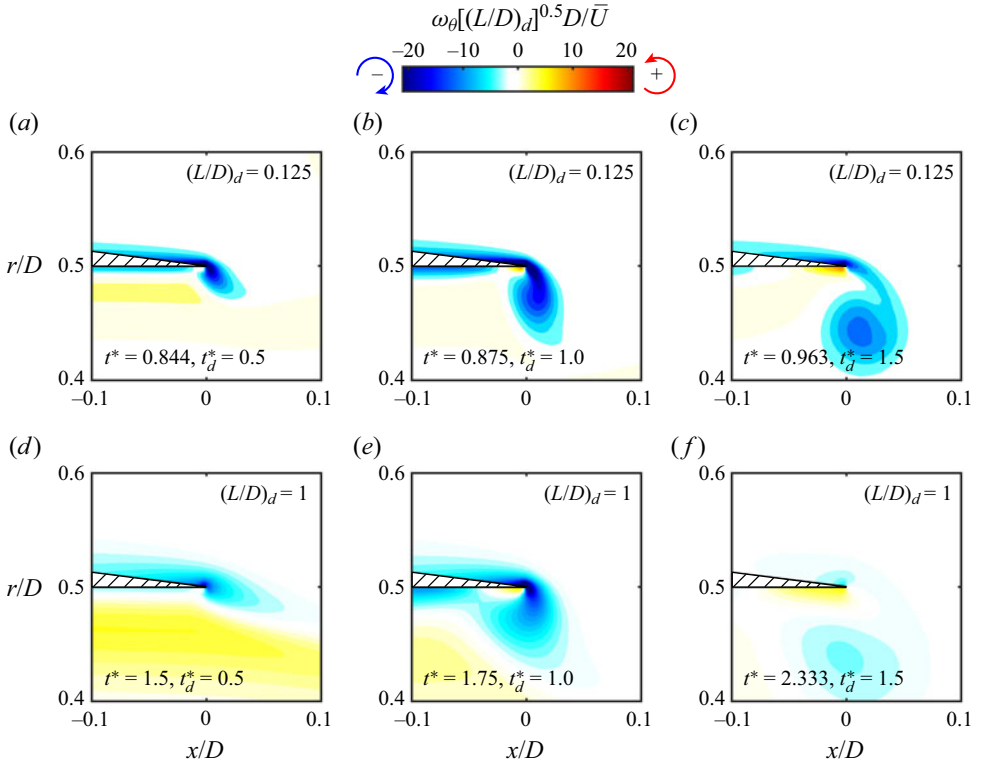

Figure 7. Azimuthal vorticity contours in x–r plane near the nozzle tip for the initial formation process of the SVR in (a–c) Case 1 with $(L/D)_d = 0.125$ and (d–f) Case 4 with $(L/D)_d = 1$ at $(L/D)_i = 0.75$.

self-induced velocity of the SVR always points upstream (indicated by the black arrow on the SVR), as shown in figures 8(b i) and 8(c i). The resulting movement is determined by the relative strength and position between the SVR and the LVR. As the radial position of vortex core decreases, the SVR moves away from the nozzle wall, weakening the positive vorticity region induced by it on the nozzle inner wall. Meantime, the vortex core of the SVR continuously absorbs vorticity from the boundary layer induced by the LVR and rearranges the vorticity distribution, thereby expanding rapidly. The mutually induced velocity from the SVR in Case 1 also causes the radial position of vortex core for the LVR to decrease (Maxworthy 1977; Das *et al.* 2017) and promotes its downstream motion (indicated by the red arrow on the LVR). The reduction in the radial position of vortex core for the LVR would also indirectly increase its self-induced velocity (Krieg & Mohseni 2021).

The corresponding temporal evolution of fluid parcels is shown in figure 8(a iii,b iii,c iii). Tracers are released into the flow at the initiation of starting jet deceleration, i.e. $t_d^* = 0$. These tracers are divided into four groups: group 1 (black for the region with $x < 0$ and $r > 0.5D$), group 2 (green for the region with $x > 0$ and $r > 0.5D$), group 3 (red for the region with $x < 0$ and $0 < r < 0.5D$) and group 4 (blue for the region with $x > 0$ and $0 < r < 0.5D$), as shown in figure 8(a iii). In the rapid accumulation stage ($t_d^* \leq 1$), the fluid tracers comprising SVR primarily originate from group 1 (figure 8b iii). The fluid entrainment from other groups is not obvious. This also shows the existence of radial

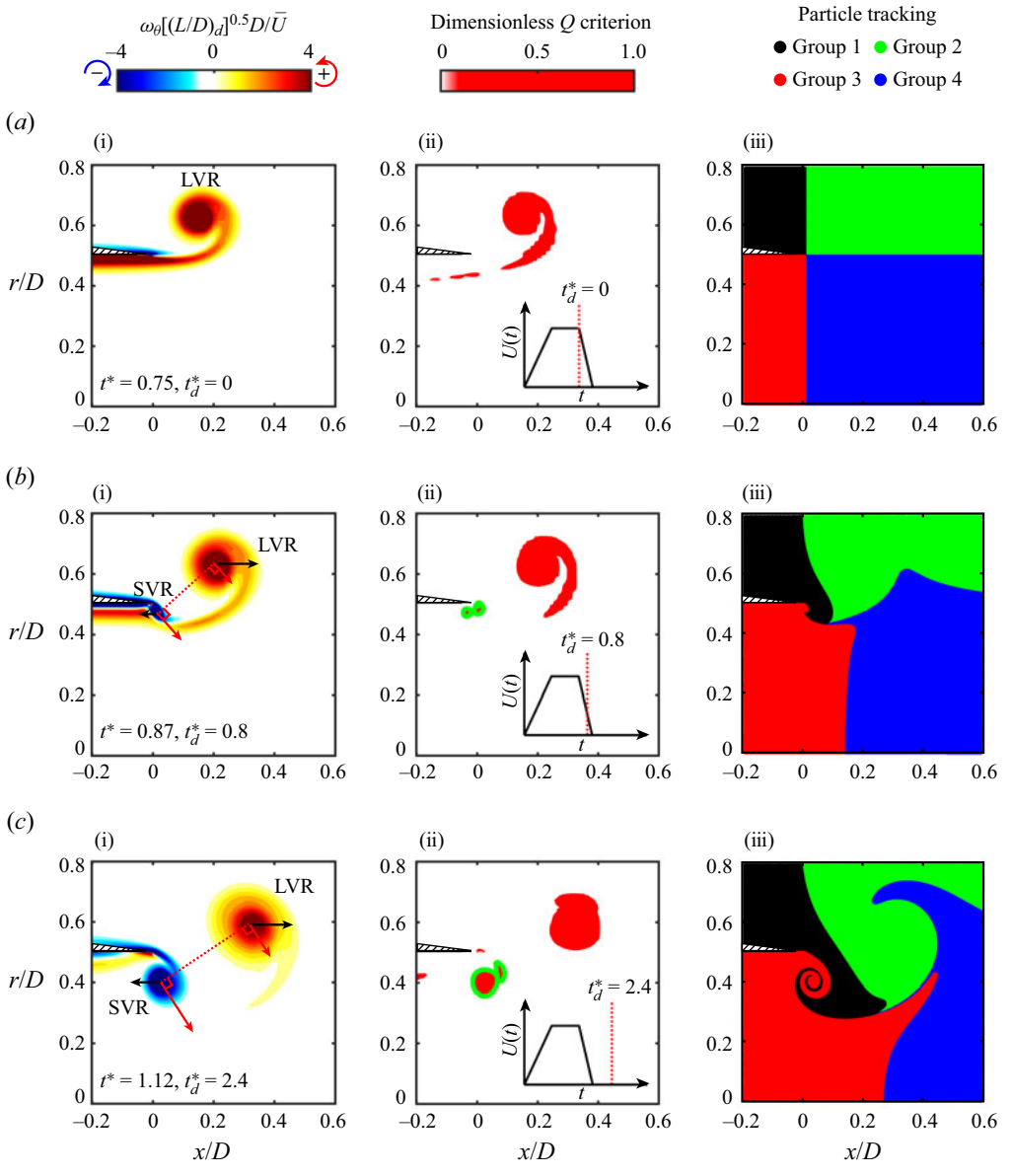

Figure 8. (i) Azimuthal vorticity contours, (ii) Q-criterion visualizations (normalized by its maximum value with regions greater than 0.05 marked in red) and (iii) temporal evolution of fluid parcels near the nozzle tip during the formation process of the SVR in Case 1 with $(L/D)_i = 0.75$ and $(L/D)_d = 0.125$. The black and red arrows in subpanels (i) represent the self-induced and mutually induced velocities on the SVR and LVR, respectively.

inward flow from the outside of the nozzle behind the formation of the SVR. During the subsequent development stage ($t_d^* > 1$), fluid tracers from group 3 are also entrained into SVR (figure 8*c* iii). The fluid tracers within SVR originate only from group 1 and group 3 with $x < 0$. The absence of entrainment of fluid tracers from group 4 can be attributed to their inherent downstream velocity upon discharge from the nozzle prior to the deceleration of the starting jet. The absence of fluid tracers from group 2 can be

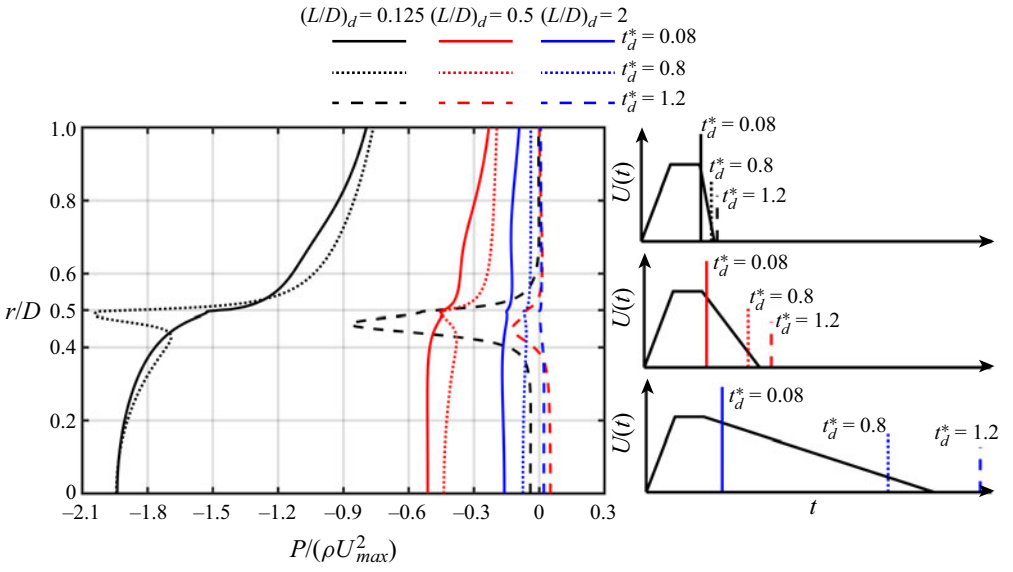

Figure 9. The instantaneous profiles of gauge pressure at the nozzle exit ($x = 0$) for Case 1 with $(L/D)_i = 0.75$ and $(L/D)_d = 0.125$, Case 3 with $(L/D)_i = 0.75$ and $(L/D)_d = 0.5$, and Case 5 with $(L/D)_i = 0.75$ and $(L/D)_d = 2$. The instants corresponding to these profiles in Cases 1, 3 and 5 are indicated on the right-hand side with the velocity programs.

explained by the induced velocity from the LVR, which causes them to move downstream faster and away from the SVR.

From the above discussion, it can be concluded that during the deceleration stage of the starting jet, there exists a radial inward flow near the nozzle exit from the outside of nozzle. This radial inward flow interacts with the nozzle wall resulting in the formation of the SVR. It is similar to the formation process of a vortex ring in the starting disk (Xu & Nitsche 2015; Steiner *et al.* 2023). Maxworthy (1977) and Didden (1979) attributed this to the induced flow produced by the LVR. However, it is important to note that the LVR produces induced flow regardless of whether the starting jet is in the deceleration stage. Nevertheless, the formation of the SVR only initiates during the deceleration stage of a starting jet. Therefore, it can be considered that, in addition to the induced flow produced by the LVR, there must be another factor driving the fluid outside the nozzle radially inward. This factor should be crucial to the formation of the SVR.

The radial pressure gradient near the nozzle exit due to the deceleration of the starting jet may be considered as the additional factor. The profiles of gauge pressure at the nozzle exit for cases with different durations of the deceleration stage, i.e. different $(L/D)_d$, are shown in figure 9. It can be observed that a radial pressure gradient forms between the inner and outer sides of the nozzle during the deceleration stage ($t_d^* = 0.08$ and $t_d^* = 0.8$). This can be attributed to the negative gauge pressure within the nozzle exit caused by the deceleration of the starting jet (Gao *et al.* 2020). After a period of deceleration, an additional low-pressure region emerges near the nozzle wall ($r = 0.5D$), i.e. at $t_d^* = 0.8$, which corresponds to the low-pressure region induced by the formed SVR (Schlueter-Kuck & Dabiri 2016). After the termination of deceleration stage, i.e. at $t_d^* = 1.2$, the radial pressure gradient disappears, and only the low-pressure region induced by SVR remains. Furthermore, as the duration of the deceleration stage increases, the rate of deceleration decreases, which in turn weakens the negative gauge pressure due to the deceleration of

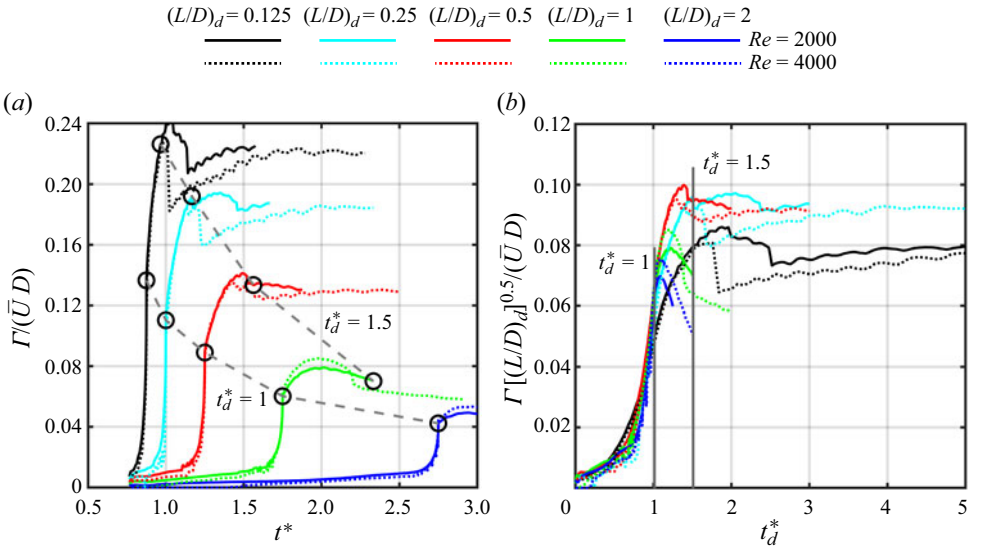

Figure 10. Circulation of the SVR against (*a*) t^* and (*b*) t_d^* for Cases 1-5 ($Re = 2000$) and Cases 15-19 ($Re = 4000$) with $(L/D)_i = 0.75$, where $(L/D)_d$ ranges from 0.125 to 2.

starting jet (Gao *et al.* 2020). This is also reflected in figure 9, where the radial pressure gradient decreases as $(L/D)_d$ increases. As the radial pressure gradient decreases, the weakening of the formed SVR leads to a corresponding weakening of the low-pressure region induced by it.

The circulation growth processes of the SVR, calculated by (2.8), are shown in figure 10 for cases with $(L/D)_i = 0.75$ and $(L/D)_d$ ranging from 0.125 to 2. Similar to the LVR (Rosenfeld *et al.* 1998; Gao 2011; Zhu *et al.* 2023*b*), the circulation growth processes of the SVR are also independent of Re (figure 10*a*). In addition, the circulation growth rate and the final circulation value of the SVR decrease as $(L/D)_d$ increases, which is consistent with the previous qualitative results. It can be found that the relationship between the final circulation of the SVR and $(L/D)_d$ can be approximately expressed as $\Gamma \sim [(L/D)_d]^{-0.5}$. To unify the circulation values of the SVR at different $(L/D)_d$, $[(L/D)_d]^{-0.5}$ should be taken into account for normalizing the circulation. For instance, the circulation can be normalized by $\bar{U}D[(L/D)_d]^{-0.5}$. On the other hand, the duration of the circulation growth of the SVR increases with increasing $(L/D)_d$, with the major part occurring during the deceleration stage of the starting jet, i.e. $0 < t_d^* \leq 1$. The duration of the circulation growth of the SVR can be approximated as T_d, although some may extend until $t_d^* = 1.5$ for small $(L/D)_d$. The circulation growth of the SVR after $t_d^* = 1$ can be attributed to the continuous absorption of negative vorticity near the nozzle exit generated during the deceleration stage of the starting jet. Of course, the additional contribution from the induced flow generated by the LVR near the nozzle exit cannot be neglected for cases with small $(L/D)_i$ and $(L/D)_d$. Considering the equation for the newly defined formation time t_d^* in the present work, i.e. (2.7), t_d^* may be more suitable than the traditional t^* to illustrate the circulation growth process of the SVR. The circulation growth processes are also shown in figure 10(*b*) as $\Gamma[(L/D)_d]^{0.5}/(\bar{U}D) \sim t_d^*$. It can be found that the circulation growth

processes with different $(L/D)_d$ collapse into a cluster of curves, i.e.

$$\frac{\mathrm{d}\{\Gamma[(L/D)_d]^{0.5}/(\bar{U}D)\}}{\mathrm{d}t_d^*} = \text{const.} \tag{3.1}$$

Introducing (2.7) into the above equation in place of t_d^*, it can be obtained that

$$\frac{\mathrm{d}\{\Gamma[(L/D)_d]^{0.5}/(\bar{U}D)\}}{\mathrm{d}[(t - T_a - T_c)/T_d]} = \text{const.}, \tag{3.2}$$

where $\bar{U}$, D, T_a and T_c can be approximately regarded as constants for the same $(L/D)_i$ and Re, and only T_d changes with $(L/D)_d$ with $T_d \sim (L/D)_d$. Equation (3.2) can then be rewritten as

$$\frac{\mathrm{d}\Gamma}{\mathrm{d}t} \sim [(L/D)_d]^{-1.5}. \tag{3.3}$$

Therefore, the circulation growth rate of the SVR $\mathrm{d}\Gamma/\mathrm{d}t$ can be scaled with $[(L/D)_d]^{-1.5}$ to unify it across different $(L/D)_d$.

3.2. *Influence from the LVR*

In order to analyse the influence from the LVR to the formation of the SVR, cases with larger $(L/D)_i = 2.25$ are chosen for comparison. In these cases, the LVR has been positioned far away from the nozzle exit at $t_d^* = 0$, resulting in a weaker induced flow generated by it near the nozzle exit (recall figure 6). The azimuthal vorticity contours and Q-criterion visualizations for Case 6 with $(L/D)_i = 2.25$ are shown in figure 11. At $t_d^* = 0$, comparing with Case 1 with $(L/D)_i = 0.75$ (recall figure 8*a* i), figure 11(*a* i) reveals that the LVR has almost exited the region of $x \leq 0.6D$, resulting in a weaker and almost negligible secondary boundary layer. As the starting jet decelerates, similar to Case 1 with $(L/D)_i = 0.75$, SVR with highly concentrated vorticity is formed near the nozzle tip during the initial rapid accumulation stage (figures 11*b* i and 11*b* ii). In the subsequent development stage, the vortex core area of the SVR expands by continuously absorbing vorticity from the boundary layer on the outer side of the nozzle and rearranging the vorticity, as shown in figures 11(*c* i) and 11(*c* ii). However, the difference from Case 1 with $(L/D)_i = 0.75$ is that, as the mutually induced velocity from the LVR diminishes, the vortex core position of the SVR remains almost unchanged near the nozzle tip. The SVR continues to induce positive vorticity on the inner wall of nozzle, which would weaken SVR through the cancellation of vorticity (James & Madnia 1996; Zhu *et al.* 2022). The temporal evolution of fluid parcels shown in figure 11(*a* iii,*b* iii*c* iii,) illustrates the influence of the LVR on the fluid entrainment during the formation of SVR. It can be observed that as the LVR translates away from the nozzle exit, fluid from group 2, in addition to the previously identified fluids from groups 1 and 3, would also be entrained into SVR, as shown in figures 11(*b* iii) and 11(*c* iii).

Comparing figures 8 and 11, one obvious variation is that the influence of the LVR on the vortex core trajectories of the SVR changes as $(L/D)_i$ increases. This is particularly evident in the radial position development of the vortex core, where the vortex core position of the SVR can be determined by the negative vorticity peak in the vortex core. The radial position development of vortex core for the SVR is shown in figure 12 for cases with both $(L/D)_i = 0.75$ and $(L/D)_i = 2.25$, where $(L/D)_d$ ranges from 0.125 to 2. In the rapid accumulation stage ($t_d^* \leq 1$), the negative vorticity peak remains near the nozzle tip ($x = 0$,

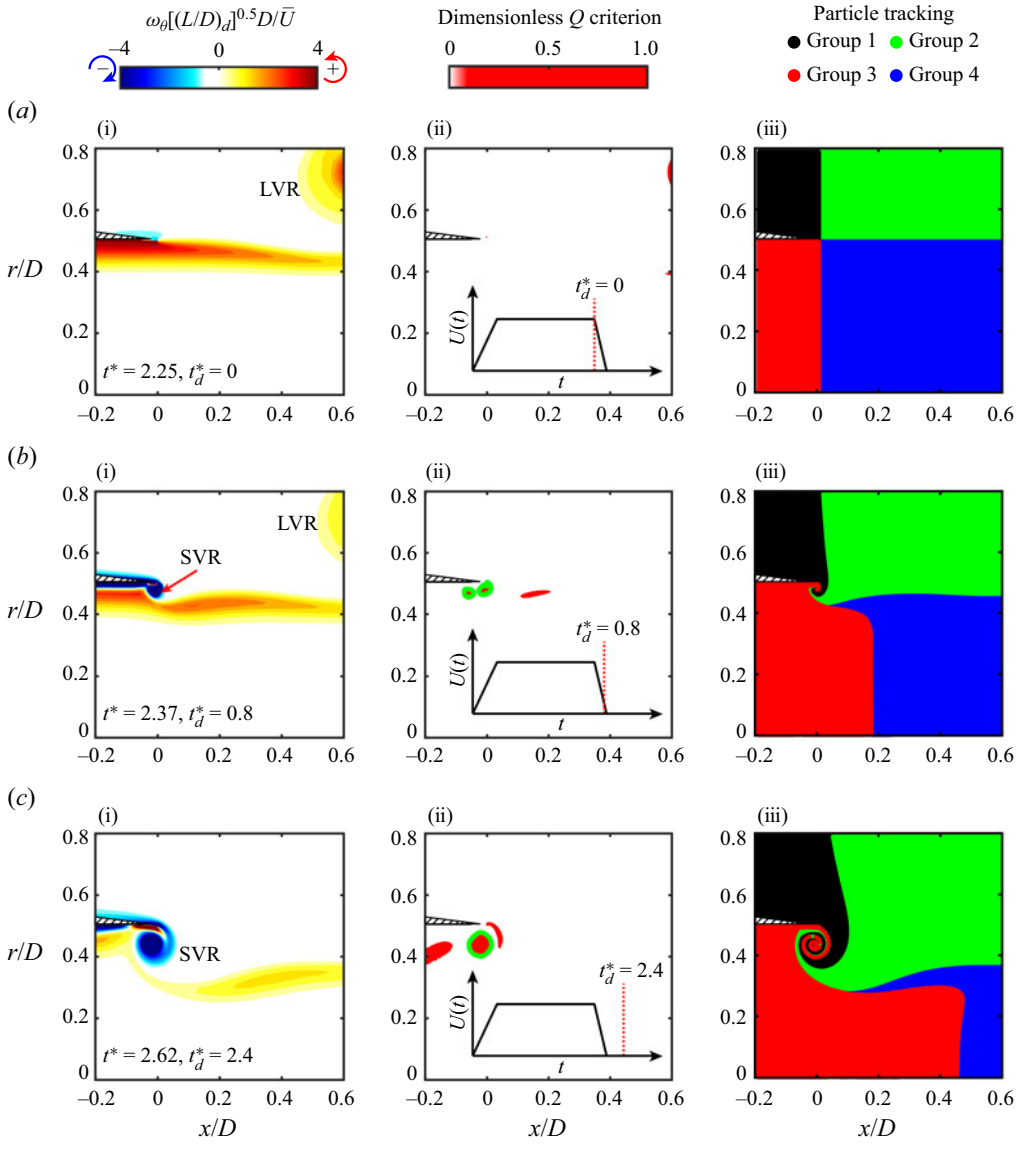

Figure 11. Azimuthal vorticity contours (i), Q-criterion visualizations (ii) and temporal evolution of fluid parcels (iii) near the nozzle tip during the formation process of the SVR in Case 6 with $(L/D)_i = 2.25$ and $(L/D)_d = 0.125$.

$r = 0.5D$), so that this stage is excluded from the present comparison. As the flow develops with increasing t_d^*, the radial position of vortex core for SVR decreases for all cases. This reduction can be attributed to two factors: the expanding vortex core area during the development stage is constrained by the nozzle wall, and the induced velocity from the LVR moves the vortex core of the SVR towards the symmetry axis ($r = 0$). Therefore, for $(L/D)_d$ equal to 0.125, 0.25 and 0.5, the reduction rate in the radial position of vortex core for the SVR is higher at $(L/D)_i = 0.75$, comparing with that at $(L/D)_i = 2.25$. As for $(L/D)_d = 1$ and 2, the rate of reduction in the radial position between different $(L/D)_i$ is almost the same. This is because, even with a smaller $(L/D)_i$, the LVR is still far away from

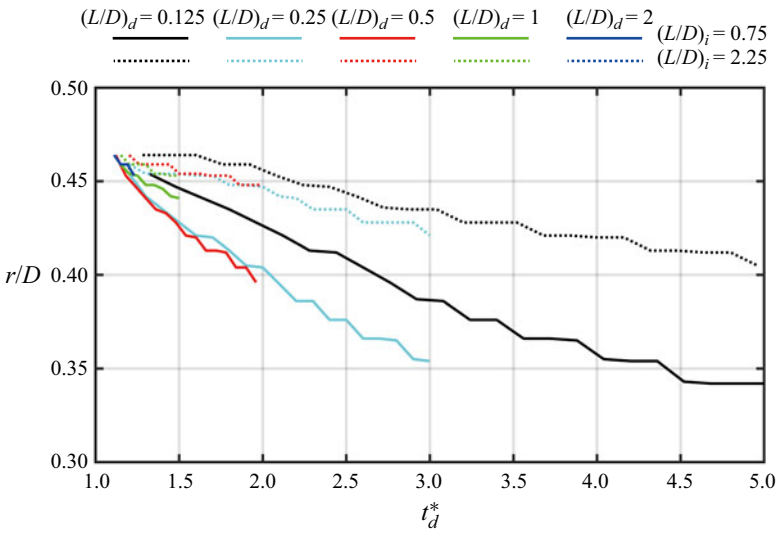

Figure 12. Comparison of Cases 1–5 with $(L/D)_i = 0.75$ and Cases 6–10 with $(L/D)_i = 2.25$ about the radial position development of vortex core for the SVR at $Re = 2000$.

the nozzle exit at $t_d^* > 1$ after the deceleration stage with a larger $(L/D)_d$, thereby losing its effective influence on SVR. Furthermore, the rapid decrease in the circulation of the SVR immediately after reaching its peak when $(L/D)_d$ is relatively large at $(L/D)_i = 0.75$ (recall figure 10*b*) can be explained by the aforementioned radial position development of the vortex core for the SVR. With a large $(L/D)_d$, SVR remains near the nozzle wall due to its losing the mutually induced velocity from the LVR, and weakens further through the typical 'vortex–wall' interaction (Orlandi & Verzicco 1993; Zhu *et al.* 2022).

The influence from the LVR on the formation of the SVR is further analysed by the circulation growth shown in figure 13 for cases with $(L/D)_i = 2.25$. The weakening of the influence from the LVR does not qualitatively alter the circulation growth process of the SVR. The conclusion obtained at $(L/D)_i = 0.75$ that the final circulation value and circulation growth rate of the SVR can be scaled by $[(L/D)_d]^{-0.5}$ and $[(L/D)_d]^{-1.5}$, respectively, can still be found in figure 13 for cases with $(L/D)_i = 2.25$. In addition, through the detailed comparison of figures 10 and 13, it can be seen that weakening the influence from the LVR has two effects on the circulation growth process of the SVR. Firstly, at $(L/D)_i = 2.25$, the maximum circulation of the SVR is approximately 10 % lower than that at $(L/D)_i = 0.75$. This suggests that the induced flow formed by the LVR and the possibly trailing vortex near the nozzle exit (Maxworthy 1977; Didden 1979) indeed promotes the formation of the SVR. Recalling figure 6, it is evident that as $(L/D)_i$ increases from 0.75 to 2.25, the induced flow formed by the LVR and the possibly trailing vortex near the nozzle exit is weakened far more than the decrease in the maximum circulation of SVR. This further confirms that the pressure difference caused by the deceleration of the starting jet, which is dominated by $(L/D)_d$, is mainly responsible for the formation of the SVR. Secondly, after the rapid growth, the circulation of the SVR either increases slowly ($(L/D)_d = 0.125$ and 0.25) or almost remains unchanged ($(L/D)_d = 0.5$) at $(L/D)_i = 0.75$, whereas it decreases continuously for all $(L/D)_d$ at $(L/D)_i = 2.25$. This can be attributed to the fact that SVR is being unable to move away from the nozzle wall when the induced velocity from the LVR is eliminated, resulting

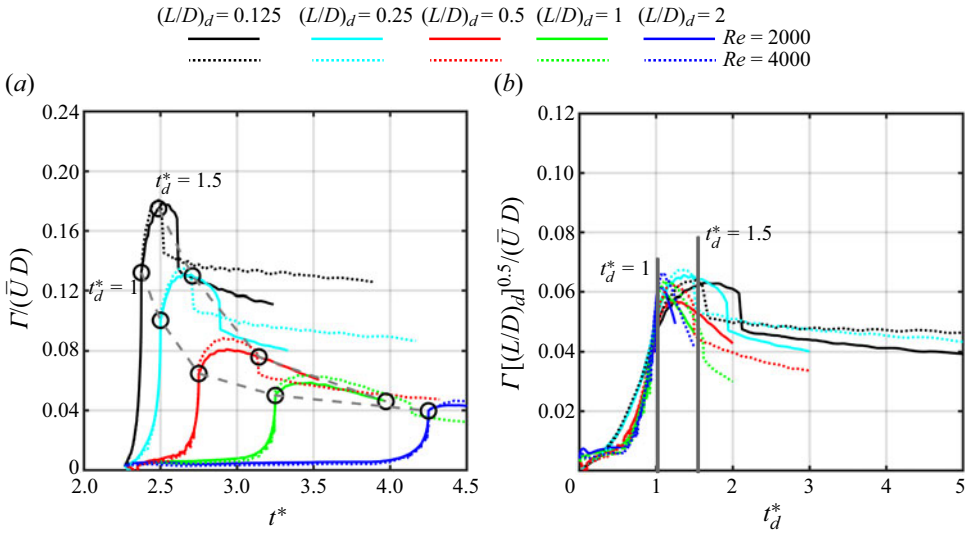

Figure 13. Circulation of the SVR against (*a*) t^* and (*b*) t_d^* for Cases 6–10 ($Re = 2000$) and Cases 20–24 ($Re = 4000$) with $(L/D)_i = 2.25$, where $(L/D)_d$ ranges from 0.125 to 2.

in continuous 'vortex–wall' interaction and a subsequent decrease in circulation (recall figure 11*c* i). In addition, the loss of the induced flow formed by the LVR and the possibly trailing vortex would also be responsible for this.

Under the influence of the LVR, the secondary boundary layer with negative vorticity (same as that in SVR) is enhanced. This may be a crucial section in the influence of the LVR on the formation of the SVR. In order to explore the role of the secondary boundary layer during the formation process of the SVR, a vertical wall is added in the nozzle exit plane, i.e. the nozzle with a tip angle of 90°, as shown in figure 2(*b*). This configuration allows the induced flow to generate a stronger secondary boundary layer (Irdmusa & Garris 1987; Gharib *et al.* 1998; Rosenfeld *et al.* 1998).

The azimuthal vorticity contours and Q-criterion visualizations for Case 11 with the vertical wall are shown in figure 14. Comparing with Case 1 without the vertical wall at $t_d^* = 0$ (recall figure 8*a* i), figure 14(*a* i) reveals that the secondary boundary layer indeed becomes more pronounced, with a portion of it being directly entrained by the LVR. At $t_d^* = 0.8$ (within the rapid accumulation stage), SVR with highly concentrated vorticity is formed near the nozzle tip (figures 14*b* i and 14*b* ii). Furthermore, a portion of negative vorticity from the vicinity of the SVR is being entrained by the LVR at this time (figure 14*b* i). During the development stage, i.e. $t_d^* > 1$, the vortex core area of the SVR expands by continuously absorbing vorticity from the secondary boundary layer and rearranging the vorticity (figures 14*c* i and 14*c* ii). Comparing figures 8(*c* i) and 14(*c* i) reveals that, due to the obstruction of the vertical wall, SVR does not move downstream under the influence of the LVR, and the reduction in the radial position of the vortex core for the SVR is also less pronounced. The radial position of the vortex core for the LVR is significantly reduced and it translates away from the nozzle exit slowly. This allows the induced velocity from the LVR to continuously enhance the secondary boundary layer and transport more negative vorticity to SVR. The fluid entrainment process of the SVR in the case with the vertical wall is qualitatively changed. The fluid particles in group 1 ($x < 0$ and $r > 0.5D$), originally entrained by SVR (recall figure 8*c* iii), are completely

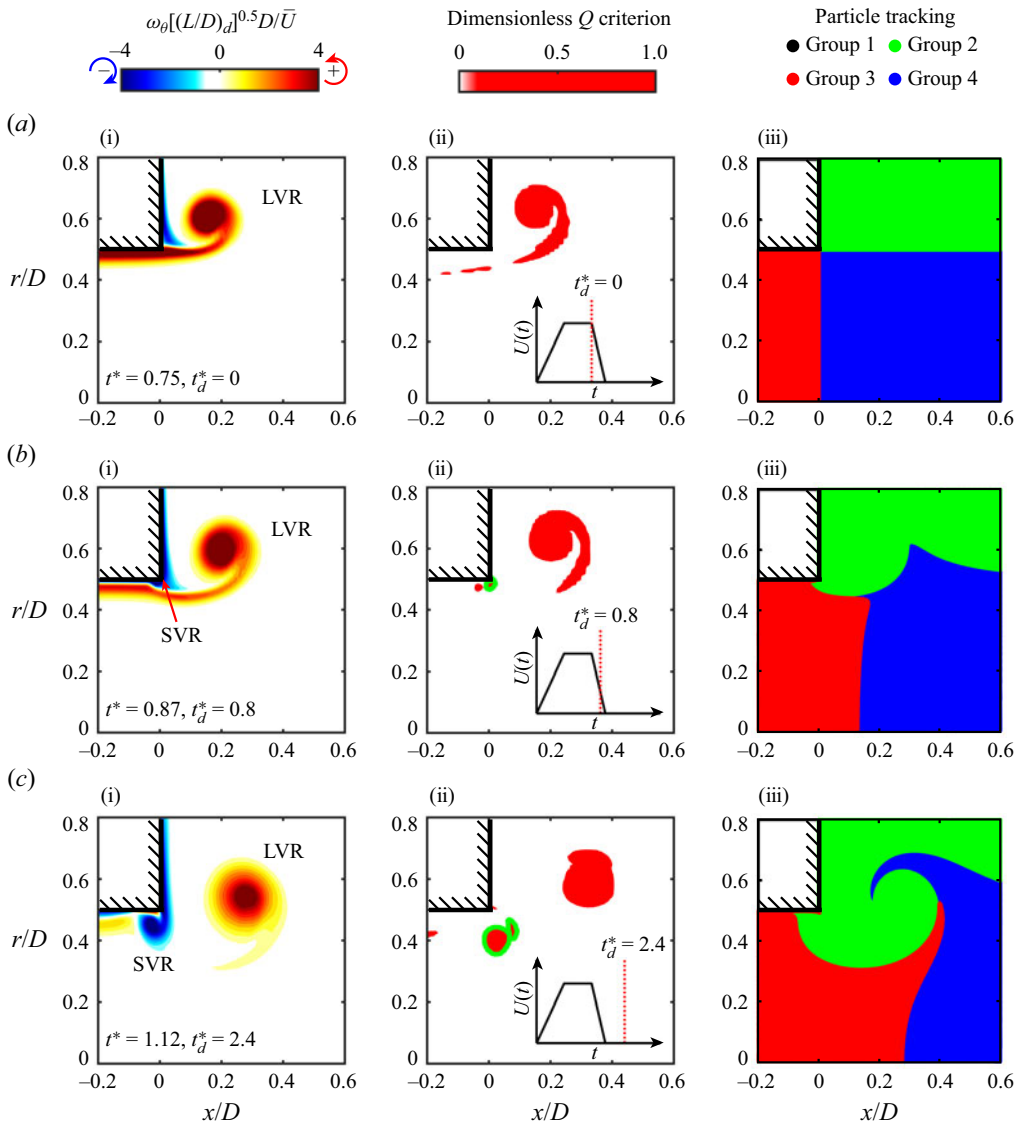

Figure 14. Azimuthal vorticity contours (i), Q-criterion visualizations (ii) and temporal evolution of fluid parcels (iii) near the nozzle tip during the formation process of the SVR in Case 11 with the vertical wall at $(L/D)_i = 0.75$ and $(L/D)_d = 0.125$.

shielded, as shown in figure 14(*a* iii). On the contrary, the fluid particles in group 2 ($x > 0$ and $r > 0.5D$), which cannot be entrained into SVR in the case without the vertical wall, expands radially inward and upstream to form SVR (see figures 14*a* iii and 14*b* iii). In addition, the ability of the SVR to entrain the fluid from group 3 ($x < 0$ and $0 < r < 0.5D$) has almost been eliminated, and almost all the fluid that constitutes SVR comes from group 2 (figure 14*c* iii).

The circulation growth processes of the SVR with different $(L/D)_i$ and $(L/D)_d$ are shown in figure 15 to quantitatively analyse the influence from the secondary boundary layer. Due to the variation in geometry, the circulation of the SVR formed

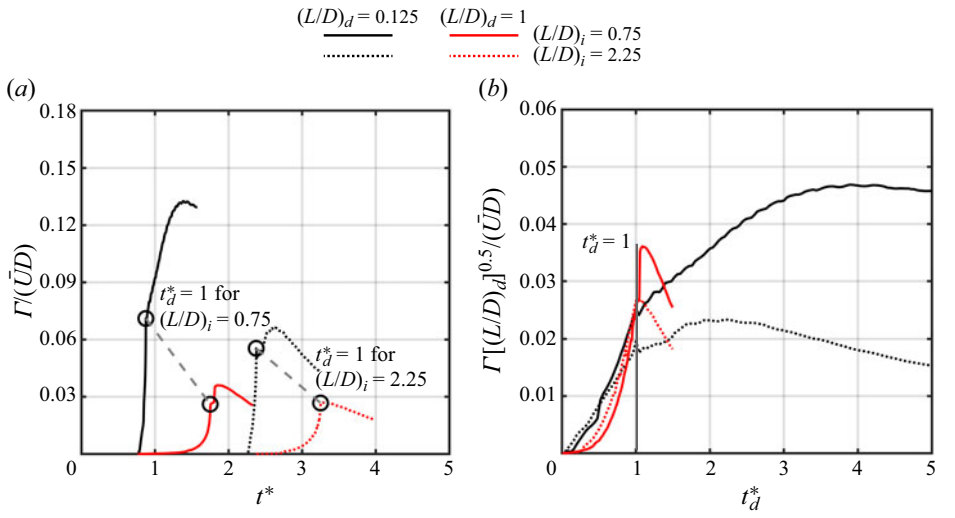

Figure 15. Circulation of the SVR in the cases with the vertical wall for Case 11 with $(L/D)_d = 0.125$ and Case 12 with $(L/D)_d = 1$ at $(L/D)_i = 0.75$, as well as Case 13 with $(L/D)_d = 0.125$ and Case 14 with $(L/D)_d = 1$ at $(L/D)_i = 2.25$ against (*a*) t^* and (*b*) t_d^*.

by the nozzle with a vertical wall is significantly reduced. However, the relationship $\Gamma[(L/D)_d]^{0.5}/(\bar{U}D) \sim t_d^*$ still collapses into a cluster of curves for different $(L/D)_d$, as shown in figure 15(*b*). This reflects that the conclusion that the final circulation value and circulation growth rate of SVR can be scaled by $[(L/D)_d]^{-0.5}$ and $[(L/D)_d]^{-1.5}$, respectively, remains valid. It can also be found from the red lines in the figure that the LVR would move away and cannot effectively affect the flow near the nozzle exit at larger $(L/D)_d$, resulting in a convergence of circulation growth processes at different $(L/D)_i$. Only when $(L/D)_d$ is small, are there differences between the circulation growth processes with different $(L/D)_i$ (see the black lines). The difference with different $(L/D)_i$ mainly occurs after $t_d^* = 1$. This can be explained by the fact that for $t_d^* < 1$, the diameter of the LVR is large, so that its induced velocity cannot effectively transport the negative vorticity from the secondary boundary layer to SVR. On the contrary, the LVR entrains part of the negative vorticity, which offsets the enhancement to the secondary boundary layer due to its induced velocity, as shown in figure 14(*b* i). As the diameter of the LVR gradually decreases after $t_d^* = 1$, its induced velocity could enhance the transport of negative vorticity from the secondary boundary layer to SVR (figure 14*c* i). For cases with a vertical wall, combining with the induced velocity from the LVR, the influence of the LVR increases the circulation of the SVR by 50 % as $(L/D)_i$ decreases from 2.25 to 0.75 (see the black lines in figure 15). This increment is much greater than the 10 % observed in the cases without a vertical wall (comparing figures 10 and 13).

4. Role of the SVR in the development of starting jet

4.1. *Influence to the development of starting jet*

4.1.1. *Leading vortex ring*

The influence of the SVR on the LVR can be considered by examining the radial position development of vortex core for LVR (Blondeaux & De Bernardinis 1983; Das *et al.* 2017). However, this has not been quantitatively analysed in conjunction with the formation

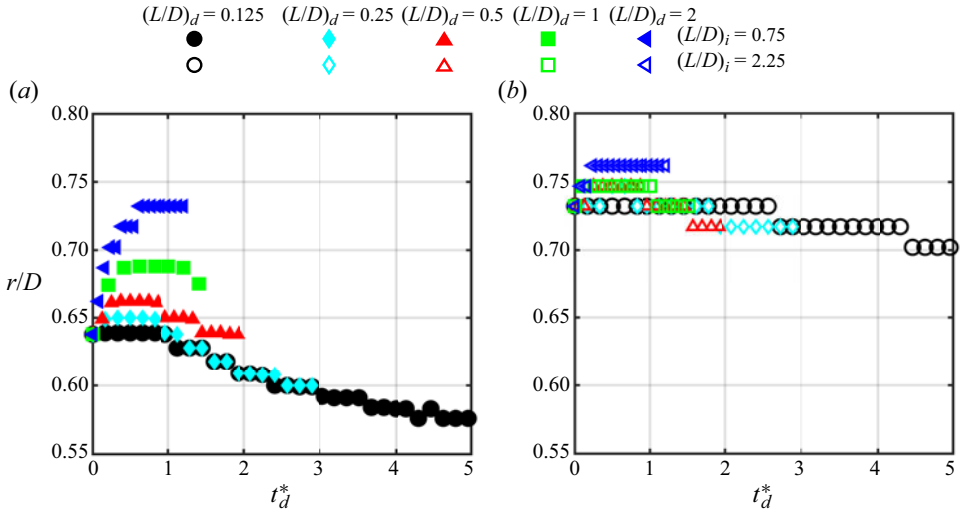

Figure 16. Radial position development of vortex core for the LVR during and after the deceleration of starting jet in (*a*) Cases 1–5 with $(L/D)_i = 0.75$ and (*b*) Cases 6–10 with $(L/D)_i = 2.25$.

process of the SVR. The radial position development of vortex core for the LVR are shown in figure 16. For $(L/D)_i = 0.75$, three types of variations are shown for different $(L/D)_d$. First, the radial position of vortex core only reduces for $(L/D)_d = 0.125$; second, the radial position of vortex core increases initially and then reduces for $(L/D)_d = 0.25$, 0.5 and 1; and finally, the radial position of vortex core only increases for $(L/D)_d = 2$ (figure 16*a*). As $(L/D)_i$ increases from 0.75 to 2.25, the radial position of vortex core for the LVR becomes larger after a longer period of growth, but with a weaker decreasing trend, comparing figures 16(*a*) and 16(*b*). The radial position of vortex core for the developing LVR is primarily influenced by several factors. Growth through the absorption of vorticity in the early stage (Gao & Yu 2010) and interaction with the trailing vortex in the later stage (Gao *et al.* 2008) both contribute to an increase in the radial position. Conversely, only the induced velocity from the SVR reduces the radial position of vortex core for LVR. Therefore, as shown in figure 16, it is evident that as SVR weakens or the LVR moves away from the nozzle exit, the decreasing trend in the radial position of vortex core for the LVR is correspondingly weakened. In addition, the decrease in the radial position of vortex core for the LVR usually starts near $t_d^* = 1$, i.e. close to the completion of the rapid accumulation stage. This can be attributed to the fact that SVR has not yet established its own induced velocity field before this instant (Zhu *et al.* 2022), and the LVR is still able to absorb the vorticity from the trailing jet and grow.

The influence of the SVR on the development of dynamic characteristics, i.e. the circulation, for the LVR is to be discussed. The circulation development processes of the LVR, calculated using (2.8) (without applying the negative sign after integration), are shown in figure 17 after the deceleration of starting jet in Cases 1–10 with different $(L/D)_i$ and $(L/D)_d$. The SVR reduces the ability of the LVR to absorb vorticity from the trailing jet. It should be noted that for two starting jets with different $(L/D)_i$ (but the same $(L/D)_d$), the velocity program after deceleration would be the same. This means that the trailing jet formed after deceleration should have similar characteristics, particularly in the distribution of vorticity flux. In cases with larger $(L/D)_i$, the LVR is closer to saturation and therefore has a weaker capacity to absorb vorticity (Krieg & Mohseni 2021).

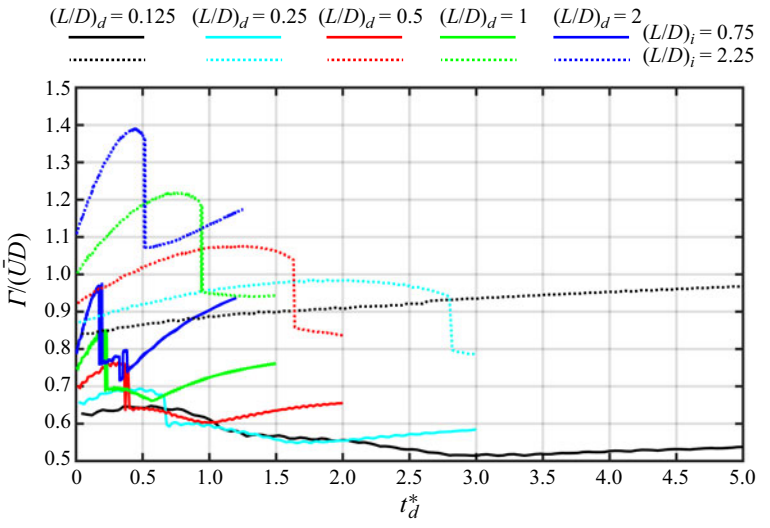

Figure 17. Circulation development of LVR during and after the deceleration stage of starting jet in Cases 1–5 with $(L/D)_i = 0.75$ and Cases 6–10 with $(L/D)_i = 2.25$.

However, as shown in figure 17, the circulation growth rate of the LVR is actually lower in cases with $(L/D)_i = 0.75$ than that in cases with $(L/D)_i = 2.25$. Even in cases with $(L/D)_d = 0.125$ and $(L/D)_d = 0.25$ at $(L/D)_i = 0.75$, the circulation of LVR decreases in the later stages of development. This can be attributed to two underlying mechanisms. First, the induced velocity from the SVR transports a portion of the nearby vorticity upstream (Wakelin & Riley 1997), away from the LVR, thereby reducing the vorticity flux that the trailing jet can supply. This might also cause the circulation of LVR to decrease due to the stripping of its vorticity when the distance between the SVR and the LVR is small enough. Secondly, the presence of the SVR alters the relative radial position between the trailing shear layer and the LVR, mainly by reducing the radial position of the former more. Inspecting figures 8(*b* i), 11(*b* i) and 11(*c* i), it can be observed that the presence of the SVR significantly reduces the radial position of the nearby trailing shear layer. This directly reduces the radial position of the trailing shear layer at the tail of the LVR for a shorter trailing jet at a smaller $(L/D)_i$. This reduction in the radial position has been considered in the investigations on the pinch-off of the LVR (Mohseni, Ran & Colonius 2001; Allen & Naitoh 2005; Dabiri & Gharib 2005), which would have weakened the ability of the LVR to absorb vorticity from the trailing shear layer. In addition, for $(L/D)_d = 0.25$, 0.5, 1 and 2 at $(L/D)_i = 2.25$ and $(L/D)_d = 0.5$, 1 and 2 at $(L/D)_i = 0.75$, there is a step reduction in the circulation of the LVR in the later stage of its development. This can be attributed to the formation of a trailing vortex in the trailing shear layer that strips away the vorticity from the LVR (Gao *et al.* 2008). The most obvious evidence is that this step reduction occurs earlier in the case with smaller $(L/D)_i$, where the ability of the LVR to absorb vorticity is weakened. The faster vorticity accumulation in the trailing shear layer and the larger relative thickness of the trailing shear layer (caused by the smaller radial position) lead to the earlier formation of the trailing vortex (Zhao, Frankel & Mongeau 2000; Gao & Yu 2012). In addition, the above-mentioned effect of the SVR on suppressing the absorption of vorticity by the LVR and even stripping vorticity from the LVR can also be manifested by the influence of the trailing vortex on the LVR (Gao *et al.* 2008; Gao

2011). It can be found that these phenomena of weakening the LVR are more obvious at $(L/D)_i = 0.75$ than at $(L/D)_i = 2.25$. Recalling figure 8, the trailing vortex cannot be generated at $(L/D)_i = 0.75$ with $(L/D)_d = 0.125$, but the circulation of the LVR in figure 17 still decreases. In addition, the decrease in the circulation growth rate of the LVR with decreasing $(L/D)_i$ also occurs in the stage before the formation of the trailing vortex, i.e. before the instant of the circulation step reduction. This effectively distinguishes the influence of the SVR from that of the trailing vortex. Therefore, it can be considered that the weakening of the circulation growth process and even the phenomenon of circulation reduction shown in figure 17 can be caused by SVR.

4.1.2. *Trailing jet*

As the LVR travels downstream, the trailing jet connecting it to the nozzle exit emerges and becomes a significant feature in the development of a starting jet (Gharib *et al.* 1998; Gao & Yu 2010; Krieg & Mohseni 2021). The trailing jet interacts with SVR near the nozzle exit. A critical characteristic of the trailing jet, i.e. the instantaneous axial distribution of vorticity flux (Gao & Yu 2012) calculated by

$$\frac{\mathrm{d}\Gamma}{\mathrm{d}t}(x) = \int_0^\infty \omega_\theta(x, r)u(x, r)\,\mathrm{d}r, \tag{4.1}$$

is shown in figure 18(*a*). The analysis is performed for the starting jet during and after the deceleration stage at $(L/D)_i = 2.25$ with $(L/D)_d = 0.125$ and 2. The absence of the results for the smaller $(L/D)_i = 0.75$ can be attributed to the limited travel distance of the LVR, which results in a relatively short and challenging-to-identify trailing jet. Based on the maximum point and the local minimum point near the tail of the LVR of vorticity flux, the vortex core position of LVR and the boundary between the LVR and the trailing jet are marked, respectively (Gao & Yu 2012). Different from the axially uniform distribution of vorticity flux in the trailing jet of a starting jet with constant velocity (figure 7 in Gao & Yu (2012)), there is a decrease in the vorticity flux distribution along the axial direction upstream towards the nozzle exit, with the vorticity flux near the nozzle exit ($x = 0$) continuously decreasing. The decreasing slope is steeper for $(L/D)_d = 0.125$. In addition, at the same t_d^* (lines with the same colour), the vorticity flux near the nozzle exit in case with $(L/D)_d = 2$ (dashed line) is slightly higher than that with $(L/D)_d = 0.125$ (solid line). Even at $t_d^* = 0.9$ and 1.2, before and after the termination of the starting jet, the vorticity flux near the nozzle exit becomes negative in case with $(L/D)_d = 0.125$.

The vorticity flux at the nozzle exit is equal to the circulation growth rate of the total starting jet, which is related to the profiles of velocity and pressure at the nozzle exit from the Helmholtz vorticity transport equation (Krieg & Mohseni 2013; Zhu *et al.* 2023*a*). The development of vorticity flux at the nozzle exit is shown in figure 18(*b*), along with the results calculated by the slug model (Gharib *et al.* 1998). The velocity programs of Case 6 and Case 10, with the same $(L/D)_i$, should be identical before the initiation of deceleration, but the development of circulation growth rates in these two cases differs. This is mainly because the different $(L/D)_d$ values result in variations in the $\bar{U}$ used to normalize the results. Before the initiation of deceleration at A, the slug model underestimates the circulation growth rate due to the presence of over pressure (Krueger 2005; Zhu *et al.* 2023*a*). Especially during the acceleration stage, the circulation growth rate reaches its peak at the end of acceleration. This underestimation persists during the deceleration stage, especially for the case with $(L/D)_d = 2$. The presence of the SVR has a positive effect on the circulation growth rate. The presence of the SVR can be

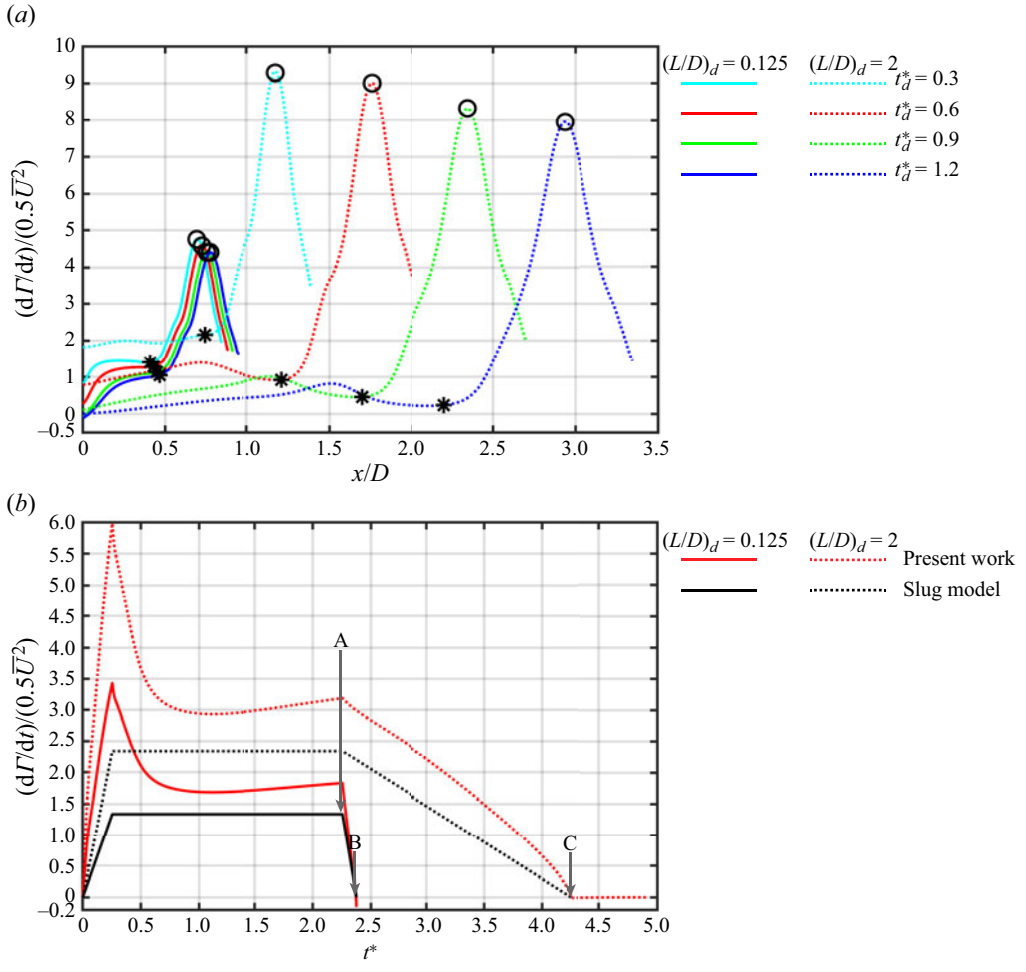

Figure 18. (*a*) The instantaneous axial distribution of vorticity flux. The star marks the boundary between the LVR and the trailing jet, while the circle denotes the vortex core position of the LVR. (*b*) The development of vorticity flux at the nozzle exit in Case 6 with $(L/D)_d = 0.125$ and Case 10 with $(L/D)_d = 2$ at $(L/D)_i = 2.25$, where A represents the initiation of deceleration, while B and C represent the termination of starting jets with $(L/D)_d = 0.125$ and $(L/D)_d = 2$, respectively.

equivalent to an obstacle that reduces the effective outward flow area of the starting jet at the nozzle exit (Zhu *et al.* 2024), which is comparable to the influence of the starting jet produced by an orifice configuration (Zhu *et al.* 2023*a*). As a result, the pressure and velocity within the nozzle exit are elevated, both contributing to the increase in circulation growth rate. It should be noted that the deceleration of the starting jet produces negative gauge pressure at the nozzle exit (Gao *et al.* 2020), which would reduce the circulation growth rate. The negative gauge pressure becomes more obvious as $(L/D)_d$ decreases, so the underestimation of the circulation growth rate by the slug model can be almost ignored during the deceleration stage in the case with $(L/D)_d = 0.125$. On the other hand, the induced velocity from the SVR transports a portion of the trailing jet shear layer upstream, thereby reducing the circulation growth rate (Wakelin & Riley 1997). This may explain why the circulation growth rate in the case with $(L/D)_d = 0.125$ becomes negative near and after the termination of the starting jet, i.e. near B.

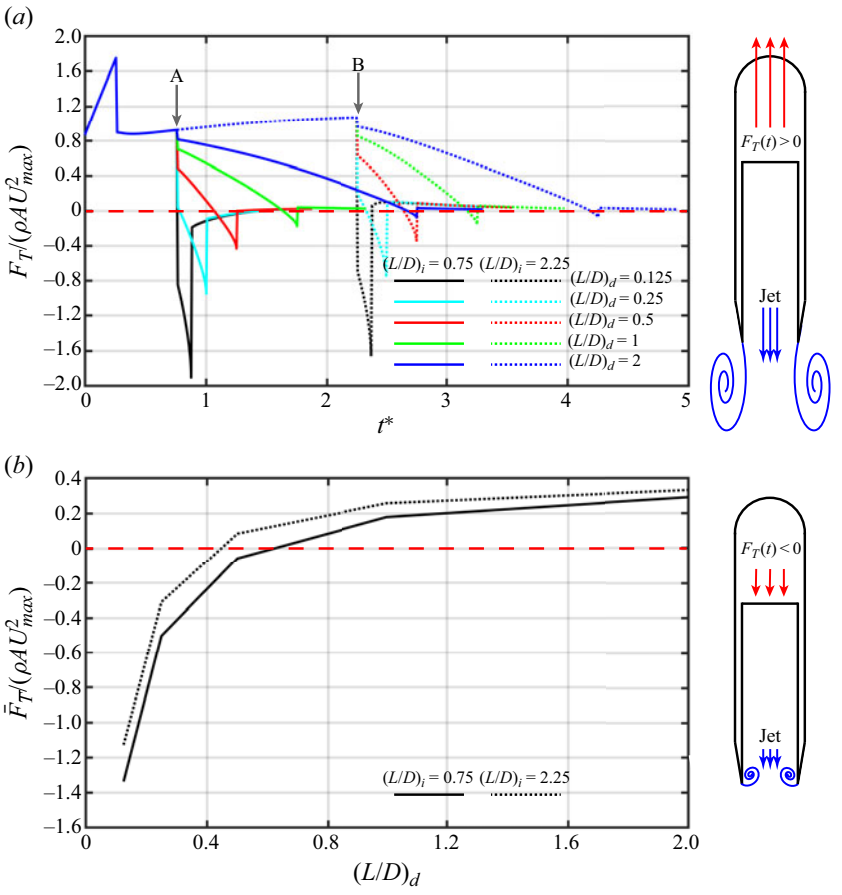

Figure 19. (*a*) The development of total thrust $F_T(t)$ generated by starting jets and (*b*) the average value of total thrust $\bar{F}_T$ during the deceleration stage for Cases 1–10 with different $(L/D)_i$ and $(L/D)_d$, where A and B represent the initiation of deceleration for $(L/D)_i = 0.75$ and $(L/D)_i = 2.25$, respectively. The red dashed lines indicate the line of zero thrust.

4.2. *Effects on the propulsive performance of starting jet after deceleration*

The propulsive performance of starting jets varies with different $(L/D)_i$ and $(L/D)_d$ during the deceleration stage, and this can be analysed through the generation of thrust. The development of total thrust $F_T(t)$ is shown in figure 19(*a*), as in Krueger & Gharib (2003), Gao *et al.* (2020) and Zhang *et al.* (2020), calculated based on the profiles of axial velocity $u(r, t)|_{x=0}$ and gauge pressure $P(r, t)|_{x=0}$ at the nozzle exit, i.e.

$$F_T(t) = \int_{r=0}^{r=D/2} 2\pi r[\rho u^2(r, t)|_{x=0} + P(r, t)|_{x=0}]\,\mathrm{d}r. \tag{4.2}$$

As shown on the right-hand side of figure 19, $F_T(t)$ is either positive or negative when the propeller receives thrust opposite to (required for propulsion) or in the same direction as the starting jet, respectively. Both the outward $(u(r, t)|_{x=0} > 0)$ and inward $(u(r, t)|_{x=0} < 0)$ flows at the nozzle exit contribute positively to $F_T(t)$ because, through control volume analysis, they both increase the momentum within the control volume containing the external fluid in the same direction as the starting jet. This contributes to the positive $F_T(t)$. There is also a definition of sign for the second term on the right-hand side of (4.2),

which is determined by the gauge pressure $P(r, t)|_{x=0}$. When the pressure at the nozzle exit is greater than the ambient pressure, $P(r, t)|_{x=0}$ is positive and contributes positively to $F_T(t)$, and *vice versa*. Before the initiation of deceleration for $(L/D)_i = 0.75$ (at A), $F_T(t)$ is the same for all cases. Subsequently, $F_T(t)$ in cases with $(L/D)_i = 0.75$ exhibits a step reduction, while in cases with $(L/D)_i = 2.25$, it continues to increase until B and then exhibits the step reduction. The continuous increase of $F_T(t)$ during the constant velocity stage has also been found in Zhang *et al.* (2020) for an impulsive starting jet with $L/D = 6$ (figure 13*b* in Zhang *et al.* (2020)). The influence of different $(L/D)_i$ on $F_T(t)$ is the same as that in Gao *et al.* (2020) for the thrust contributed by pressure in the starting jets with different velocity programs. The thrust contributed by pressure is the second term on the right-hand side of (4.2), referred to as pressure thrust, $F_P(t)$. For velocity program transitioning later from the constant velocity stage to the deceleration stage, $F_P(t)$ can continue to increase for a longer time. Due to the downstream translation of the LVR, its effect of inducing low pressure near the nozzle exit is weakened, resulting in an increase in $F_P(t)$ (Gao *et al.* 2020). This is responsible for the continuous increase of $F_T(t)$ during the constant velocity stage. For smaller $(L/D)_i$, the earlier deceleration induces negative gauge pressure, resulting in a negative $F_P(t)$. Consequently, $F_T(t)$ with $(L/D)_i = 0.75$ first exhibits a step reduction.

For both $(L/D)_i = 0.75$ and 2.25, $F_T(t)$ starts to bifurcate at the initiation of deceleration due to different $(L/D)_d$. During the deceleration stage, which ends with a step rise, $F_T(t)$ decreases monotonically. The magnitudes of the step reduction at the initiation and the step rise at the termination both decrease with increasing $(L/D)_d$. Furthermore, $F_T(t)$ is consistently negative for cases with $(L/D)_d \leq 0.25$. In contrast, for cases with $(L/D)_d > 0.25$, $F_T(t)$ transitions from positive to negative as the starting jet slows down, and it remains positive overall at $(L/D)_d = 2$ due to the sufficiently small rate of deceleration. After the termination of the starting jet, the flow near the nozzle exit is dominated by SVR, and $F_T(t)$ continues to develop further. For cases with $(L/D)_d \leq 0.25$ and $(L/D)_i = 0.75$, in which the LVR has a significant influence on the formation process of the SVR, $F_T(t)$ remains negative for a period of time. Otherwise, $F_T(t)$ is close to or slightly greater than 0 under the action of the SVR. The average value of $F_T(t)$ during the deceleration stage $\bar{F}_T$ is illustrated in figure 19(*b*). Deceleration in general is unfavourable for the generation of thrust. As the rate of deceleration increases, i.e. decreasing $(L/D)_d$, $\bar{F}_T$ decreases. Even, for the smaller $(L/D)_d = 0.125$ and 0.25, $\bar{F}_T$ is less than 0. As $(L/D)_i$ increases from 0.75 to 2.25, the generation of $F_T(t)$ is enhanced for all $(L/D)_d$, i.e. the larger $\bar{F}_T$. This increment decreases as $(L/D)_d$ increases. The total thrust $F_T(t)$ can be decomposed into the velocity thrust component $F_U(t)$ and the pressure thrust component $F_P(t)$ based on the two terms on the right-hand side of (4.2), i.e.

$$F_U(t) = \int_{r=0}^{r=D/2} 2\pi r \rho u^2(r, t)|_{x=0}\, \mathrm{d}r, \tag{4.3}$$

$$F_P(t) = \int_{r=0}^{r=D/2} 2\pi r P(r, t)|_{x=0}\, \mathrm{d}r. \tag{4.4}$$

The development of $F_U(t)$ and $F_P(t)$ are shown in figure 20 after the initiation of deceleration. During the deceleration stage, $F_U(t)$ decreases monotonically and is almost identical for different $(L/D)_i$ and $(L/D)_d$ at the initial stage, but the differences become apparent as the starting jet decelerates and SVR grows (figure 20*a*). Overall, $F_U(t)$ increases with increasing $(L/D)_i$ from 0.75 to 2.25 and the decrease of $(L/D)_d$, which corresponds to the weakening of the influence from the LVR and the enhancement of the SVR, respectively. After the termination of the starting jet, due to the induced flow from

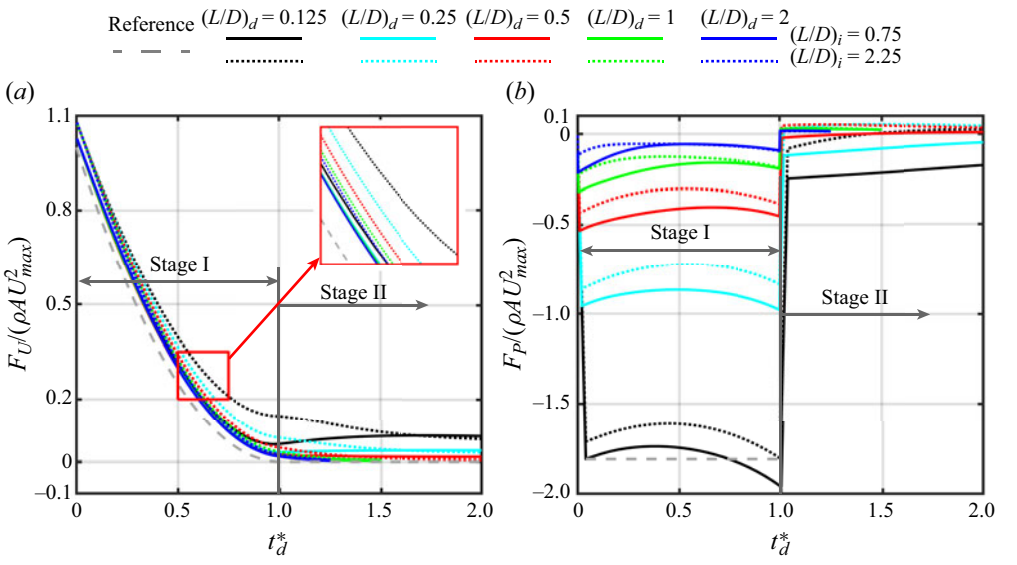

Figure 20. The development of (*a*) velocity thrust $F_U(t)$ and (*b*) pressure thrust $F_P(t)$ generated by the starting jet after the initiation of deceleration for Cases 1–10 with different $(L/D)_i$ and $(L/D)_d$. Stages I and II correspond to the deceleration stage ($0 < t_d^* \leq 1$) and the termination stage ($t_d^* > 1$) of starting jet, respectively.

the SVR at the nozzle exit, $F_U(t)$ always remains positive with a non-negligible magnitude. Comparing with the results calculated based on the slug model (indicated by the grey dashed line in figure 20*a*), the disturbance to $u(r, t)|_{x=0}$ by SVR caused an increase by at least 10 % in the average value of $F_U(t)$ during the deceleration stage. The slug model assumes that the velocity at nozzle exit is uniform and exactly equal to the velocity of starting jet (Didden 1979; Gharib *et al.* 1998; Zhu *et al.* 2022).

In comparison, the variation of $(L/D)_i$ and $(L/D)_d$ has a greater influence on $F_P(t)$ than on $F_U(t)$. Moreover, $F_P(t)$ shows significant variations with respect to $(L/D)_d$ during $0 < t_d^* \leq 1$ (figure 20*b*). The gauge pressure at the nozzle exit is negative due to the deceleration of starting jet and further diminishes with increasing the rate of deceleration (Gao *et al.* 2020). Therefore, $F_P(t)$ diminishes as $(L/D)_d$ decreases with a magnitude much greater than that in $F_U(t)$. This is responsible for the decrease in $\bar{F}_T$ as $(L/D)_d$ decreases in figure 19(*b*). As $(L/D)_i$ increases from 0.75 to 2.25, $F_P(t)$ shows an overall increase for small $(L/D)_d$, while it only increases in the early stage and then remains the same for large $(L/D)_d$. This also explains the observed increase in $\bar{F}_T$ as $(L/D)_i$ increases, but the magnitude of increment decreases with increasing $(L/D)_d$ (recall figure 19*b*). At the instant of the termination of starting jet, there is a step rise in $F_P(t)$ for all cases due to no longer decelerating and generating negative gauge pressure. After the termination of the starting jet, $F_P(t)$ remains negative for a longer duration for $(L/D)_d \leq 0.25$ with $(L/D)_i = 0.75$ (stage II in figure 20*b*), which results in negative $F_T(t)$.

Re-examining $F_P(t)$ during the deceleration stage, it is negative since $P(r, t)|_{x=0}$ is dominated by the deceleration of the starting jet in each case. The negative gauge pressure at the nozzle exit should be related to the rate of deceleration (Zhu *et al.* 2023*a*). However, for the constant deceleration rate in the present work, $F_P(t)$ still increases at first ($0 < t_d^* < 0.5$) and then decreases ($0.5 < t_d^* < 1$) during the deceleration stage. This can be attributed to the disturbance caused by the formation of the SVR. In general, SVR is beneficial to the generation of $F_P(t)$ during the deceleration stage. To quantitatively

calculate the influence of the SVR on $F_P(t)$, it can be assumed as a reference that there is no process in which $F_P(t)$ increases at first ($0 < t_d^* < 0.5$) and then decreases ($0.5 < t_d^* < 1$). The reference based on the above assumptions for calculating the influence of the SVR on $F_P(t)$ is inserted as a grey dashed line in figure 20(*b*). For simplicity, the reference is given only for Case 1 with $(L/D)_i = 0.75$ and $(L/D)_d = 0.125$. By designating the constant pressure thrust, assuming without the influence of the SVR, as F_{P_ref}, the variation in the average value of $F_P(t)$ during the deceleration stage caused by the formation of the SVR can be calculated as follows:

$$\Delta\bar{F}_P = \frac{\displaystyle\int_{T_a+T_c}^{T_a+T_c+T_d} [F_P(t) - F_{P\_ref}]\,\mathrm{d}t}{T_d}, \tag{4.5}$$

where F_{P_ref} can be approximately selected as $F_P(t)$ at the initial instant when the starting jet has entered the deceleration stage but the influence of the SVR can still be ignored. When $\Delta\bar{F}_P$ is positive, it means that SVR has a positive influence on the generation of $F_P(t)$. After calculation, $\Delta\bar{F}_P$ varies from $0.02\rho AU_{max}^2$ to $0.13\rho AU_{max}^2$ for starting jets with different $(L/D)_i$ and $(L/D)_d$. Furthermore, the deceleration of the starting jet reduces the average value of $F_P(t)$ during the deceleration stage by the magnitude of F_{P_ref}. However, the formation of the SVR could reduce the magnitude of the negative $F_P(t)$, expressed as a ratio as follows:

$$\eta = \frac{\Delta\bar{F}_P}{|F_{P\_ref}|}. \tag{4.6}$$

After calculation, η varies from 1 % to 60 % for starting jets with different $(L/D)_i$ and $(L/D)_d$. Therefore, it can be considered that the formation of the SVR compensates for approximately 1 % to 60 % of the reduction in $F_P(t)$ caused by the deceleration.

The instantaneous axial velocity profiles $u(r,t)|_{x=0}$ and gauge pressure profiles $P(r,t)|_{x=0}$ at the nozzle exit are shown in figures 21 and 22 to discuss the relationship between the propulsive performance and the influence from the vortical structures. The existence of the SVR is beneficial for the generation of $F_U(t)$. It can be seen from figure 21(*a*) that the induced flow from the SVR directly changes $u(r,t)|_{x=0}$. On one hand, the induced flow transports the external fluid into the nozzle, corresponding to the region of $u(r,t)|_{x=0} < 0$. By control volume analysis, this increases the momentum within the control volume containing the external fluid in the same direction as the starting jet, contributing positive $F_U(t)$. On the other hand, due to the fixed volume inside the nozzle, this portion of inward fluid needs to be discharged by the region of $u(r,t)|_{x=0} > 0$ into the control volume containing the external fluid. This is equivalent to increasing the mass flux discharged by the starting jet and also contributes positively to $F_U(t)$. This benefit becomes more pronounced as $(L/D)_i$ increases from 0.75 to 2.25, with the higher velocity magnitude for both the negative and positive $u(r,t)|_{x=0}$. For smaller $(L/D)_i = 0.75$, the induced velocity from the LVR, which has not yet moved away from the nozzle exit, carries SVR downstream (recall figure 8*b* i). The SVR is then offset from the nozzle exit, diminishing the influence of the induced flow from it. As the starting jet approaches termination or completely terminates, the flow near the nozzle exit is dominated by the induced flow from the SVR. The SVR transports external fluid back into the nozzle (Gao *et al.* 2020). An equal amount of fluid should be discharged due to continuity, as observed at $t_d^* = 1.1$ in figure 21(*b*). Both the flow entering and discharging through the nozzle produce positive $F_U(t)$ by increasing the momentum within the control volume containing the external fluid in the same direction as the starting jet. This can explain why $F_U(t)$

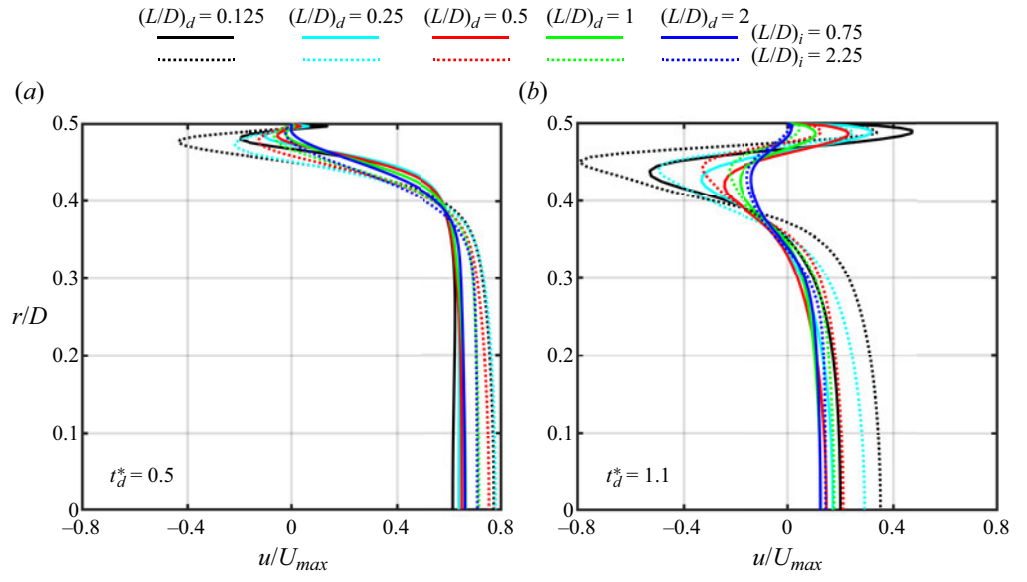

Figure 21. The instantaneous profiles of axial velocity at the nozzle exit $u(r, t)|_{x=0}$ for (*a*) $t_d^* = 0.5$ and (*b*) $t_d^* = 1.1$ in Cases 1–10 with different $(L/D)_i$ and $(L/D)_d$.

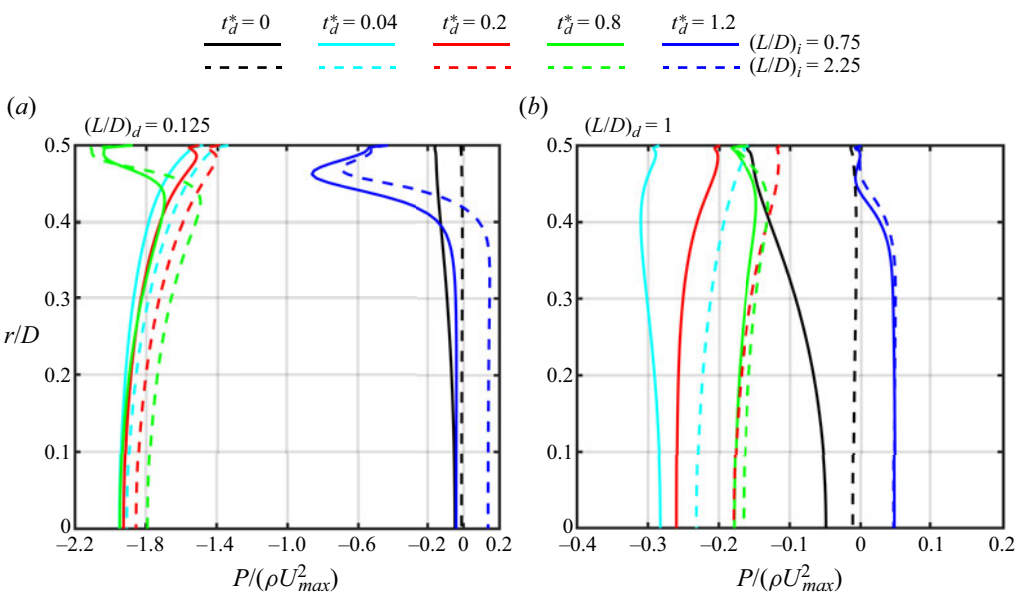

Figure 22. The development of gauge pressure profiles at the nozzle exit $P(r, t)|_{x=0}$ for (*a*) Cases 1 and 6 at $(L/D)_d = 0.125$ and (*b*) Cases 4 and 9 at $(L/D)_d = 1$ but with different $(L/D)_i$.

remains positive with a non-negligible magnitude after the termination of starting jet (recall figure 20*a*).

Shifting our attention to the development of gauge pressure profiles at the nozzle exit $P(r, t)|_{x=0}$ that produces $F_P(t)$, as shown in figure 22 for five critical instants in cases with different $(L/D)_d$ and $(L/D)_i$. The cases with different $(L/D)_i$ at small $(L/D)_d$ are

compared in figure 22(*a*). When the starting jet has not yet begun to decelerate at $t_d^* = 0$, it can be observed that for $(L/D)_i = 2.25$, $P(r, t)|_{x=0}$ is entirely 0, while it is below 0 for $(L/D)_i = 0.75$. This is because, for $(L/D)_i = 0.75$, the LVR is not far away from the nozzle exit and induces low pressure there. Therefore, $F_P(t)$ produced at $(L/D)_i = 2.25$ is always larger than that at $(L/D)_i = 0.75$ during the deceleration stage at small $(L/D)_d$ (recall figure 20*b*). As the deceleration of the starting jet occurs, $P(r, t)|_{x=0}$ decreases rapidly from close to 0 to an overall negative value with a large magnitude, as shown by the $P(r, t)|_{x=0}$ at $t_d^* = 0.04$. This corresponds to the step reduction of $F_P(t)$ immediately after $t_d^* = 0$ (recall figure 20*b*). As $P(r, t)|_{x=0}$ develops further, from $t_d^* = 0.04$ to $t_d^* = 0.2$, it shows an overall increase. This can be associated with the formation of the SVR, which causes the starting jet to converge at the nozzle exit. The reduction in the outflow area of starting jet leads to its acceleration, requiring an additional pressure difference to drive the process (Krieg & Mohseni 2013; Zhu *et al.* 2023*a*, 2024). The gauge pressure at the nozzle exit thus increases. As a result, $F_P(t)$ generated increases during $t_d^* < 0.5$. However, SVR also induces a low pressure region as a vortical structure (Schlueter-Kuck & Dabiri 2016; Gao *et al.* 2020) that expands as it develops, shown by the region near the nozzle wall ($r = 0.5D$) of $P(r, t)|_{x=0}$ at $t_d^* = 0.8$. Therefore, $F_P(t)$ decreases during $0.5 < t_d^* < 1$ because the low pressure induced by the SVR offsets the pressure increase caused by the reduction in outflow area and dominates. In general, the existence of the SVR is beneficial for the generation of $F_P(t)$ during the deceleration stage, although only for a short period of improvement. After the termination of the starting jet at $t_d^* = 1.2$, the negative gauge pressure caused by deceleration disappears, and $P(r, t)|_{x=0}$ is only dominated by SVR. The induced velocity from the SVR tends to transport fluid back into the nozzle, but additional fluid cannot be added due to the fixed volume inside the nozzle. This results in a positive gauge pressure in the centre part of nozzle exit to repel fluid entry. For $(L/D)_d = 0.125$ with $(L/D)_i = 0.75$, the LVR moves SVR downstream (recall figure 8*b* i), weakening this process, and the pressure in the central part cannot be effectively increased. Furthermore, the LVR, which has not yet moved far away, together with SVR, induces low pressure region near the nozzle exit. Therefore, $F_P(t)$ is negative for a longer duration but continues to increase as the LVR moves away during $t_d^* > 1$. As $(L/D)_d$ increases from 0.125 to 1 shown in figure 22(*b*), the above discussion about $t_d^* = 0$, $t_d^* = 0.04$ and $t_d^* = 0.2$ remains unchanged, only the portion for $t_d^* > 0.5$ is altered. For larger $(L/D)_d = 1$, since the LVR at small $(L/D)_i$ has also moved far away from the nozzle exit after a longer duration of deceleration, the differences between $(L/D)_i = 0.75$ and $(L/D)_i = 2.25$ gradually disappear as t_d^* approaches and exceeds 1. In addition, as $(L/D)_d$ increases, indicating a longer duration of the deceleration stage, the magnitude of negative gauge pressure at the nozzle exit caused by the deceleration of starting jet also decreases.

5. Summary

The mechanisms responsible for the formation of SVR and its effects on the development of a starting jet have been systematically investigated via three-dimensional numerical simulations in the present work. Simple trapezoidal velocity programs with different $(L/D)_i$ (0.75 and 2.25) and $(L/D)_d$ (ranging from 0.125 to 2) have been used, where $(L/D)_i$ and $(L/D)_d$ are the stroke ratios of starting jet before the initiation of deceleration and during the deceleration stage, respectively.

The formation process of the SVR can be summarized into two stages based on the formation time t_d^* defined by the duration of deceleration stage T_d (see (2.7)). First

is the rapid accumulation stage ($t_d^* \leq 1$), during which the negative vorticity (opposite to the LVR) accumulates at the nozzle tip with a concentrated vorticity distribution. This is followed by the development stage ($t_d^* > 1$), where the development of the SVR rearranges the initially concentrated vorticity distribution into an approximately Gaussian distribution within the vortex core. For the same $(L/D)_i$ and $(L/D)_d$, the circulation growth of the SVR is independent of the Reynolds number Re investigated from 2000 to 4000 ($Re = \rho U_{max} D/\mu$). At the same $(L/D)_i$ but different $(L/D)_d$, the final circulation value and the circulation growth rate of the SVR can be scaled by $[(L/D)_d]^{-0.5}$ and $[(L/D)_d]^{-1.5}$, respectively.

Comparing cases with different $(L/D)_i$, it is found that, in addition to the induced flow generated by the LVR, the radial inward flow under the radial pressure difference near the nozzle exit is more important for the formation of the SVR. This radial pressure difference results from the negative gauge pressure formed at the nozzle exit due to the deceleration of starting jet. By increasing $(L/D)_i$ from 0.75 to 2.25, the LVR would be positioned farther from the nozzle exit, weakening the flow induced there when the starting jet begins to decelerate. Even though the LVR becomes stronger by absorbing more fluid and vorticity as $(L/D)_i$ increases from 0.75 to 2.25, it has been shown that the induced flow from it near the nozzle exit is weakened to a quarter, and the straining field formed by it is also being far away from the nozzle exit. The SVR can still be generated and with only a 10 % reduction in circulation.

For $(L/D)_i = 0.75$ with small $(L/D)_d$, the induced velocity from the LVR helps to shift the vortex core of the SVR downstream and towards the central axis. As a consequence, the interaction between SVR and the nozzle wall is weakened, which allows it to maintain strength for a longer duration. The fluid entrainment for SVR is investigated using the fluid tracer method, where fluid from both inside and outside the nozzle can be entrained to form SVR. However, for $(L/D)_i = 0.75$, the fluid outside the nozzle and downstream of the nozzle exit ($x > 0$ and $r > 0.5D$) would not be entrained by SVR due to the induced velocity from the LVR. Furthermore, the influence of the secondary boundary layer, which is induced by the LVR on the nozzle wall, on the formation of the SVR is also examined by adding a vertical wall at the nozzle exit. The induced velocity from the LVR enhances the secondary boundary layer and transports the negative vorticity within it to SVR, thereby further increasing the circulation of the SVR after the deceleration stage. Based on the temporal evolution of fluid parcels, it can be found that transitioning from a nozzle with a tip angle of 7° to a nozzle with a vertical wall significantly inhibits the entrainment of fluid inside the nozzle by SVR.

The influence of the SVR on the starting jet is primarily examined in two aspects: its influence on the two components that constitute the starting jet (LVR and trailing jet), as well as its effects on the most critical application characteristic of the starting jet, i.e. propulsive performance. Under the influence of the SVR, the radial position of vortex core for the LVR decreases after t_d^* approaches 1. In addition, SVR also suppresses the LVR from absorbing vorticity from the trailing shear layer and even directly strips vorticity from the LVR at small $(L/D)_i$ and $(L/D)_d$. As for the trailing jet, due to deceleration, the axial distribution of its vorticity flux decreases along the upstream direction. The presence of the SVR reduces the effective flow area of the starting jet at the nozzle exit, which in turn accelerates the starting jet and offsets the decrease in circulation growth rate caused by negative gauge pressure due to the deceleration.

Finally, for the propulsive performance of the starting jet, the existence of the SVR is beneficial for the generation of both velocity thrust component $F_U(t)$ and pressure thrust component $F_P(t)$ during the deceleration stage. The SVR affects the axial velocity profiles

$u(r, t)|_{x=0}$ and gauge pressure profiles $P(r, t)|_{x=0}$ at the nozzle exit, thereby changing the generation of $F_U(t)$ and $F_P(t)$, respectively. During the deceleration stage, SVR leads the starting jet to generate higher $F_U(t)$ by transporting external fluid into the nozzle and increasing the mass flux of fluid discharged from the nozzle. Both actions increase the momentum within the control volume containing the external fluid in the same direction as the starting jet. Meanwhile, the SVR has two effects on $P(r, t)|_{x=0}$. First, it reduces the actual outward flow area of the starting jet, causing it to converge near the nozzle exit, thereby increasing the pressure near the centre part. Second, SVR, as a vortical structure, induces low pressure region that expands as it develops. After the termination of the starting jet, $u(r, t)|_{x=0}$ and $P(r, t)|_{x=0}$ are dominated by the induced flow with zero net flow from the SVR. Here $F_U(t)$ remains positive with a non-negligible magnitude under this induced flow. The generation of $F_P(t)$ is determined by both the low pressure near the nozzle wall induced by SVR as a vortical structure and the positive gauge pressure in the centre part induced to repel fluid entry. In general, SVR can increase the average value of $F_U(t)$ during the deceleration stage by at least 10 % and compensate for approximately 1 % to 60 % of the reduction in $F_P(t)$ caused by the deceleration. Therefore, SVR enhances the total thrust generation of starting jet during the deceleration stage by increasing both components of the total thrust, $F_U(t)$ and $F_P(t)$, simultaneously.

Declaration of interests. The authors report no conflict of interest.

Author ORCIDs.
Jianwei Zhu https://orcid.org/0000-0002-5518-675X;
Lei Gao https://orcid.org/0000-0003-0377-2746.

References

Alben, S., Miller, L.A. & Peng, J. 2013 Efficient kinematics for jet-propelled swimming. *J. Fluid Mech.* **733**, 100–133.

Allen, J.J. & Naitoh, T. 2005 Experimental study of the production of vortex rings using a variable diameter orifice. *Phys. Fluids* **17** (6), 061701.

Anderson, E.J. & Grosenbaugh, M.A. 2005 Jet flow in steadily swimming adult squid. *J. Expl Biol.* **208** (6), 1125–1146.

Asadi, H., Asgharzadeh, H. & Borazjani, I. 2018 On the scaling of propagation of periodically generated vortex rings. *J. Fluid Mech.* **853**, 150–170.

Auerbach, D. 1991 Stirring properties of vortex rings. *Phys. Fluids* A **3** (5), 1351–1355.

Bi, X. & Zhu, Q. 2020 Pulsed-jet propulsion via shape deformation of an axisymmetric swimmer. *Phys. Fluids* **32** (8), 081902.

Bi, X. & Zhu, Q. 2022 Role of internal flow in squid-inspired jet propulsion. *Phys. Fluids* **34** (3), 031906.

Blondeaux, P. & De Bernardinis, B. 1983 On the formation of vortex pairs near orifices. *J. Fluid Mech.* **135**, 111–122.

Costello, J.H., Colin, S.P., Gemmell, B.J., Dabiri, J.O. & Sutherland, K.R. 2015 Multi-jet propulsion organized by clonal development in a colonial siphonophore. *Nat. Commun.* **6** (1), 8158.

Dabiri, J.O. 2009 Optimal vortex formation as a unifying principle in biological propulsion. *Annu. Rev. Fluid Mech.* **41**, 17–33.

Dabiri, J.O., Colin, S.P. & Costello, J.H. 2007 Morphological diversity of medusan lineages constrained by animal–fluid interactions. *J. Expl Biol.* **210** (11), 1868–1873.

Dabiri, J.O., Colin, S.P., Costello, J.H. & Gharib, M. 2005*a* Flow patterns generated by oblate medusan jellyfish: field measurements and laboratory analyses. *J. Expl Biol.* **208** (7), 1257–1265.

Dabiri, J.O. & Gharib, M. 2005 Starting flow through nozzles with temporally variable exit diameter. *J. Fluid Mech.* **538**, 111–136.

Dabiri, J.O., Gharib, M., Colin, S.P. & Costello, J.H. 2005*b* Vortex motion in the ocean: in situ visualization of jellyfish swimming and feeding flows. *Phys. Fluids* **17** (9), 091108.

Das, D., Bansal, M. & Manghnani, A. 2017 Generation and characteristics of vortex rings free of piston vortex and stopping vortex effects. *J. Fluid Mech.* **811**, 138–167.

DIDDEN, N. 1979 On the formation of vortex rings: rolling-up and production of circulation. *Z. Angew. Math. Phys.* **30**, 101–116.

DUCLOS, K.T., GEMMELL, B.J., COLIN, S.P., COSTELLO, J.H., DABIRI, J.O. & SUTHERLAND, K.R. 2022 Distributed propulsion enables fast and efficient swimming modes in physonect siphonophores. *Proc. Natl Acad. Sci. USA* **119** (49), e2202494119.

FERNANDO, J.N. & RIVAL, D.E. 2016 Reynolds-number scaling of vortex pinch-off on low-aspect-ratio propulsors. *J. Fluid Mech.* **799**, R3.

GAO, L. 2011 The pinch-off process of the leading vortex ring in a starting jet. PhD thesis, School of Mechanical and Aerospace Engineering, Nanyang Technological University Singapore.

GAO, L., WANG, X., YU, S.C.M. & CHYU, M.K. 2020 Development of the impulse and thrust for laminar starting jets with finite discharged volume. *J. Fluid Mech.* **902**, A27.

GAO, L. & YU, S.C.M. 2010 A model for the pinch-off process of the leading vortex ring in a starting jet. *J. Fluid Mech.* **656**, 205–222.

GAO, L. & YU, S.C.M. 2012 Development of the trailing shear layer in a starting jet during pinch-off. *J. Fluid Mech.* **700**, 382–405.

GAO, L., YU, S.C.M., AI, J.J. & LAW, A.W.K. 2008 Circulation and energy of the leading vortex ring in a gravity-driven starting jet. *Phys. Fluids* **20** (9), 093604.

GEMMELL, B.J., COSTELLO, J.H., COLIN, S.P., STEWART, C.J., DABIRI, J.O., TAFTI, D. & PRIYA, S. 2013 Passive energy recapture in jellyfish contributes to propulsive advantage over other metazoans. *Proc. Natl Acad. Sci. USA* **110** (44), 17904–17909.

GHARIB, M., RAMBOD, E. & SHARIFF, K. 1998 A universal time scale for vortex ring formation. *J. Fluid Mech.* **360**, 121–140.

GLEZER, A. 1988 The formation of vortex rings. *Phys. Fluids* **31** (12), 3532–3542.

GLEZER, A. & COLES, D. 1990 An experimental study of a turbulent vortex ring. *J. Fluid Mech.* **211**, 243–283.

DE GUYON, G. & MULLENERS, K. 2021 Scaling of the translational velocity of vortex rings behind conical objects. *Phys. Rev. Fluids* **6** (2), 024701.

HIGUCHI, H., BALLIGAND, H. & STRICKLAND, J.H. 1996 Numerical and experimental investigations of the flow over a disk undergoing unsteady motion. *J. Fluids Struct.* **10** (7), 705–719.

IRDMUSA, J.Z. & GARRIS, C.A. 1987 Influence of initial and boundary conditions on vortex ring development. *AIAA J.* **25** (3), 371–372.

JAMES, S. & MADNIA, C.K. 1996 Direct numerical simulation of a laminar vortex ring. *Phys. Fluids* **8** (9), 2400–2414.

JOHARI, H. & DESABRAIS, K.J. 2005 Vortex shedding in the near wake of a parachute canopy. *J. Fluid Mech.* **536**, 185–207.

KANG, L., GAO, A.K., HAN, F., CUI, W. & LU, X.Y. 2023 Propulsive performance and vortex dynamics of jellyfish-like propulsion with burst-and-coast strategy. *Phys. Fluids* **35** (9), 091904.

KAPLANSKI, F., SAZHIN, S.S., FUKUMOTO, Y., BEGG, S. & HEIKAL, M. 2009 A generalized vortex ring model. *J. Fluid Mech.* **622**, 233–258.

KRIEG, M. & MOHSENI, K. 2013 Modelling circulation, impulse and kinetic energy of starting jets with non-zero radial velocity. *J. Fluid Mech.* **719**, 488–526.

KRIEG, M. & MOHSENI, K. 2021 A new kinematic criterion for vortex ring pinch-off. *Phys. Fluids* **33** (3), 037120.

KRUEGER, P.S. 2005 An over-pressure correction to the slug model for vortex ring circulation. *J. Fluid Mech.* **545**, 427–443.

KRUEGER, P.S. & GHARIB, M. 2003 The significance of vortex ring formation to the impulse and thrust of a starting jet. *Phys. Fluids* **15** (5), 1271–1281.

KRUEGER, P.S. & GHARIB, M. 2005 Thrust augmentation and vortex ring evolution in a fully-pulsed jet. *AIAA J.* **43** (4), 792–801.

LE, T.B., BORAZJANI, I., KANG, S. & SOTIROPOULOS, F. 2011 On the structure of vortex rings from inclined nozzles. *J. Fluid Mech.* **686**, 451–483.

LIMBOURG, R. & NEDIĆ, J. 2021*a* An extended model for orifice starting jets. *Phys. Fluids* **33** (6), 067109.

LIMBOURG, R. & NEDIĆ, J. 2021*b* Formation of an orifice-generated vortex ring. *J. Fluid Mech.* **913**, A29.

LINDEN, P.F. & TURNER, J.S. 2004 'optimal' vortex rings and aquatic propulsion mechanisms. *Proc. R. Soc. Lond. Ser.* B **271** (1539), 647–653.

MARUGAN-CRUZ, C., RODRIGUEZ-RODRIGUEZ, J. & MARTINEZ-BAZAN, C. 2013 Formation regimes of vortex rings in negatively buoyant starting jets. *J. Fluid Mech.* **716**, 470–486.

MAXWORTHY, T. 1977 Some experimental studies of vortex rings. *J. Fluid Mech.* **81** (3), 465–495.

MOHSENI, K., RAN, H. & COLONIUS, T. 2001 Numerical experiments on vortex ring formation. *J. Fluid Mech.* **430**, 267–282.

OLCAY, A.B. & KRUEGER, P.S. 2010 Momentum evolution of ejected and entrained fluid during laminar vortex ring formation. *Theor. Comput. Fluid Dyn.* **24**, 465–482.

ORLANDI, P. & VERZICCO, R. 1993 Vortex rings impinging on walls: axisymmetric and three-dimensional simulations. *J. Fluid Mech.* **256**, 615–646.

PAWLAK, G., CRUZ, C.M., BAZÁN, C.M. & HRDY, P.G. 2007 Experimental characterization of starting jet dynamics. *Fluid Dyn. Res.* **39** (11-12), 711.

RINGUETTE, M.J., MILANO, M. & GHARIB, M. 2007 Role of the tip vortex in the force generation of low-aspect-ratio normal flat plates. *J. Fluid Mech.* **581**, 453–468.

ROSENFELD, M., RAMBOD, E. & GHARIB, M. 1998 Circulation and formation number of laminar vortex rings. *J. Fluid Mech.* **376**, 297–318.

SADRI, V. & KRUEGER, P.S. 2017 Formation and behavior of counter-rotating vortex rings. *Theor. Comput. Fluid Dyn.* **31**, 369–390.

SCHLUETER-KUCK, K. & DABIRI, J.O. 2016 Pressure evolution in the shear layer of forming vortex rings. *Phys. Rev. Fluids* **1** (1), 012501.

DA SILVA, C.B. & PEREIRA, J.C.F. 2008 Invariants of the velocity-gradient, rate-of-strain, and rate-of-rotation tensors across the turbulent/nonturbulent interface in jets. *Phys. Fluids* **20** (5), 055101.

STEINER, J., MORIZE, C., DELBENDE, I., SAURET, A. & GONDRET, P. 2023 Vortex rings generated by a translating disk from start to stop. *Phys. Rev. Fluids* **8**, 064702.

TRIELING, R.R., BECKERS, M. & VAN HEIJST, G.J.F. 1997 Dynamics of monopolar vortices in a strain flow. *J. Fluid Mech.* **345**, 165–201.

TROOLIN, D.R. & LONGMIRE, E.K. 2010 Volumetric velocity measurements of vortex rings from inclined exits. *Exp. Fluids* **48**, 409–420.

WAKELIN, S.L. & RILEY, N. 1997 On the formation and propagation of vortex rings and pairs of vortex rings. *J. Fluid Mech.* **332**, 121–139.

WEIHS, D. 1977 Periodic jet propulsion of aquatic creatures. *Front. Zool.* **24** (2-3), 171–175.

XU, L. & NITSCHE, M. 2015 Start-up vortex flow past an accelerated flat plate. *Phys. Fluids* **27** (3), 033602.

YANG, A., JIA, L. & YIN, X. 2012 Formation process of the vortex ring generated by an impulsively started circular disc. *J. Fluid Mech.* **713**, 61–85.

ZHANG, X., WANG, J. & WAN, D. 2020 Cfd investigations of evolution and propulsion of low speed vortex ring. *Ocean Engng* **195**, 106687.

ZHAO, W., FRANKEL, S.H. & MONGEAU, L.G. 2000 Effects of trailing jet instability on vortex ring formation. *Phys. Fluids* **12** (3), 589–596.

ZHU, J., ZHANG, G., GAO, L. & YU, S.C.M. 2022 The formation process of annular starting jets. *J. Fluid Mech.* **949**, A47.

ZHU, J., ZHANG, G., GAO, L. & YU, S.C.M. 2023*a* The circulation growth of non-impulsive starting jet. *Phys. Fluids* **35** (5), 057102.

ZHU, J., ZHANG, G., GAO, L. & YU, S.C.M. 2023*b* Vortex ring formation process in starting jets with uniform background co-and counter-flow. *J. Fluid Mech.* **968**, A26.

ZHU, J., ZHANG, G., XIA, H., YU, S.C.M. & GAO, L. 2024 The influence of background co-flow on the propulsive characteristics of starting jets. *Ocean Engng* **309**, 118463.